CENTRAL RESEARCH LIBRARY
DOCUMENT COLLECTION

PAH

MARTIN MARIETTA ENERGY SYSTEMS LIBRARIES
3 4456 0360634 6

ORNL 1438
Reactors – Research and Power
4A

DETERMINATION OF THE POWER OF THE BULK SHIELDING REACTOR – PART II

Neutron Flux Measurements in Several Beryllium Oxide – Reflected Critical Assemblies

E. B. Johnson and J. L. Meem

CENTRAL RESEARCH LIBRARY
DOCUMENT COLLECTION

LIBRARY LOAN COPY

DO NOT TRANSFER TO ANOTHER PERSON

If you wish someone else to see this document, send in name with document and the library will arrange a loan.

OAK RIDGE NATIONAL LABORATORY
OPERATED BY
CARBIDE AND CARBON CHEMICALS COMPANY
A DIVISION OF UNION CARBIDE AND CARBON CORPORATION
UCC
POST OFFICE BOX P
OAK RIDGE, TENNESSEE

OFFICIAL USE ONLY

the
unauthorized person is prohibited.

BM

[redacted]

ORNL-1438
This document consists of
111 pages. Copy 4 of 159
Series A

Contract No. W-7405-eng-26

DETERMINATION OF THE POWER OF THE BULK SHIELDING REACTOR--PART II NEUTRON FLUX MEASUREMENTS IN SEVERAL BERYLLIUM OXIDE--REFLECTED CRITICAL ASSEMBLIES

E. B. Johnson and J. L. Meem

Date Issued

APPROVED DECLASSIFIED

Per Letter Instructions Of
AEC 3-12-54
2-4-57 M. Shirley
For: N. T. Bray, Supervisor
Laboratory Records Dept.
ORNL

OAK RIDGE NATIONAL LABORATORY

Operated by

CARBIDE AND CARBON CHEMICALS COMPANY

A Division of Union Carbide and Carbon Corporation

Post Office Box P

Oak Ridge [redacted]

[redacted]

MARTIN MARIETTA ENERGY SYSTEMS LIBRARIES

3 4456 0360634 6

[redacted]

ORNL 1438
Reactors-Research and Power

INTERNAL DISTRIBUTION

1. C. E. Center
2. Biology Library
3. Health Physics Library
4-5. Central Research Library
6. Reactor Experimental Engineering Library
7-12. Central Files
13. C. E. Larson
14. W. B. Humes (K-25)
15. L. B. Emlet (Y-12)
16. A. M. Weinberg
17. E. H. Taylor
18. E. D. Shipley
19. A. H. Snell
20. F. C. VonderLage
21. R. C. Briant
22. J. A. Swartout
23. S. C. Lind
24. F. L. Steahly
25. A. Hollaender
26. J. H. Frye, Jr.
27. W. M. Good
28. M. T. Kelley
29. G. H. Clewett
30. R. S. Livingston
31. K. Z. Morgan
32. J. S. Felton
33. A. S. Householder
34. C. P. Keim
35. C. S. Harrill
36. C. E. Winters
37. D. S. Billington
38. D. W. Cardwell
39. E. M. King
40. E. O. Wollan
41. A. J. Miller
42. R. B. Briggs
43. L. D. Roberts
44. R. N. Lyon
45. W. C. Koehler
46. W. K. Ergen
47. E. P. Blizard
48. M. E. Rose
49. D. D. Cowen
50. W. M. Breazeale (consultant)
51. P. M. Reyling
52. G. C. Williams

EXTERNAL DISTRIBUTION

53-63. Argonne National Laboratory
64. Armed Forces Special Weapons Project (Sandia)
65-69. Atomic Energy Commission, Washington
70. Battelle Memorial Institute
71-73. Brookhaven National Laboratory
74. Bureau of Ships
75-76. California Research and Development Company
77-82. Carbide and Carbon Chemicals Company (Y-12 Plant)
83. Chicago Patent Group
84. Chief of Naval Research
85. Department of the Navy - Op 36
86-90. duPont Company
91-93. General Electric Company (ANPP)
94-97. General Electric Company, Richland
98. Hanford Operations Office
99-105. Idaho Operations Office
106. Iowa State College
107-110. Knolls Atomic Power Laboratory
111-112. Los Alamos Scientific Laboratory
113. Massachusetts Institute of Technology (Kaufmann)
114-116. Mound Laboratory

[redacted]

[redacted]

[redacted]

117. National Advisory Committee for Aeronautics, Cleveland
118. National Advisory Committee for Aeronautics, Washington
119-120. New York Operations Office
121-122. North American Aviation, Inc.
123. Nuclear Development Associates, Inc.
124. Patent Branch, Washington
125. Rand Corporation
126. San Francisco Operations Office
127. Savannah River Operations Office, Augusta
128. Savannah River Operations Office, Wilmington
129-130. University of California Radiation Laboratory
131. Vitro Corporation of America
132. Walter Kidde Nuclear Laboratories, Inc.
133-136. Westinghouse Electric Corporation
137-144. Wright Air Development Center
145-159. Technical Information Service, Oak Ridge

[redacted]

[redacted]

[redacted]

Contents

	Page
Abstract	7
Introduction	8
Critical Assemblies	9
Loading No. 2	9
Loading No. 8	9
Loading No. 9	10
Loading No. 11	13
Loading No. 15	13
Thermal-Neutron Flux Measurements and Power Calculations	14
Measurements on the Special Element	15
Results	21
Discussion of Errors	28
Acknowledgements	30
Appendix A - List of Critical Assemblies	31
Appendix B - Tabular Data	45
Appendix C - Leakage Calculations for Divided Shield Reactor	85
Appendix D - Determination of the Thermal-Neutron Flux in Slots 1 and 3 of the X-10 Standard Graphite Pile	91
Appendix E - Calibration of Counters and Foils	95
Appendix F - Linearity of Reactor Controls	100
Appendix G - Time Decay of Neutrons and Gamma Rays from the Beryllium Oxide--Reflected Reactor	105

[redacted]

[redacted]

List of Figures [redacted]

Figure		Page
1	Divided Shield Mockup with Reactor in Place.	11
2	Sketch of Reactor in Divided Shield Mockup	12
3	Special Fuel Assembly (Shows Center Fuel Plate, Removable Disks, Thermocouples and Water Tube)	16
4	Thermal-Neutron Flux Distribution on the Special Fuel Element. .	18
5	Thermal-Neutron Flux Distribution on Special Fuel Element. . . .	19
6	Variation of Cadmium Ratio with Distance from Centerline on the Special Fuel Element.	20
7	Power Distribution in the Open Water Divided Shield Reactor . . (Experiment 6 - Bulk Shielding Facility).	22
8	Power Distribution in the Divided Shield Reactor (Experiment 7)	23
9	Power Distribution in the "Offset Reactor" (Experiment 11). . .	24
10a-10b	Comparison of Power Distributions Through the Bulk Shielding Reactors	25
11	Comparison of Thermal-Neutron Flux Distributions in the Unit Shield and Divided Shield Reactor.	27
A-1	Fuel Assembly Arrangement - Critical Loading No. 1	32
A-2	Fuel Assembly Arrangement - Critical Loading No. 2	33
A-3	Fuel Assembly Arrangement - Critical Loading No. 3	34
A-4	Fuel Assembly Arrangement - Critical Loading No. 8	36
A-5	Fuel Assembly Arrangement - Critical Loading No. 8B	37

[redacted]

[redacted]

[redacted]

List of Figures (cont.)

Figure		Page
A-6	Fuel Assembly Arrangement - Critical Loading No. 9	38
A-7	Fuel Assembly Arrangement - Critical Loading No. 9D	39
A-8	Fuel Assembly Arrangement - Critical Loading No. 14.	41
A-9	Fuel Assembly Arrangement - Critical Loading No. 15.	42
A-10	Fuel Assembly Arrangement - Critical Loading No. 17.	43
A-11	Fuel Assembly Arrangement - Critical Loading No. 19.	44
C-1	P(Z) Linear Power Density as a Function of Z	88
G-1	Decay of Neutrons and Gamma Rays after Shutdown.	106
G-2	Decay of Neutrons and Gamma Rays after Shutdown.	107

[redacted]

[redacted]

List of Tables

Table		Page
B-1	Thermal-Neutron Flux Measurements in the Divided Shield Reactor (Experiment 6)	46
B-2	Thermal-Neutron Traverses Through the Divided Shield Reactor (Experiment 6)	52
B-3	Power Distribution Within the Divided Shield Reactor (Experiment 6)	56
B-4	Thermal-Neutron Flux Measurements in the Divided Shield Reactor (Experiment 7)	58
B-5	Thermal-Neutron Traverses Through the Divided Shield Reactor (Experiment 7)	62
B-6	Power Distribution Within the Divided Shield Reactor (Experiment 7)	65
B-7	Thermal-Neutron Flux Measurements in the "Offset Reactor" (Experiment 11)	67
B-8	Thermal-Neutron Traverses Through the "Offset Reactor" (Experiment 11)	75
B-9	Power Distribution Within the "Offset Reactor" (Experiment 11)	79
B-10	Thermal-Neutron Flux Data on Special Element A-74S in Position 37 (Experiment 11)	80
B-11	Thermal-Neutron Centerline Flux Measurements for Open Water Reactors	83

[redacted]

[redacted]

[redacted]

List of Tables (Cont.)

Table		Page
C-1	Leakage Calculations for Divided Shield Reactor in Water (Experiment 11)	89
C-2	Leakage Calculations for Divided Shield Reactor in Place in Divided Shield Mockup (Experiment 7)	90
D-1	Foil Data from the X-10 Standard Graphite Pile	94
F-1	Counting Rates Obtained as Power of Reactor Changes from 0.1 to 10^4 watts	102
F-2	Counting Rates Obtained as Power of Reactor Changes from 10 to 10^5 watts	104

[redacted]

[redacted]

[redacted]

Abstract

The power of the Bulk Shielding Reactor with a beryllium oxide reflector has been determined for several critical assemblies. The determinations were made by measuring the thermal-neutron flux distribution throughout the reactor. Several experiments of interest in the operation of a "swimming pool" type reactor are described in the appendices.

DETERMINATION OF THE POWER OF THE BULK SHIELDING REACTOR--PART II*

NEUTRON FLUX MEASUREMENTS IN SEVERAL BERYLLIUM OXIDE--REFLECTED CRITICAL ASSEMBLIES

E. B. Johnson and J. L. Meem

Introduction

A method for determining the power of the Bulk Shielding Reactor was described in an earlier report(1) hereinafter referred to as Part I. This reactor was water-reflected on all sides except the rear, where the permanent beryllium oxide reflector was located, and was used for the measurements made on the unit shield mockup. Subsequently the reactor has been used in several other critical assemblies, all of which have been beryllium oxide--reflected on four sides. This report describes the power determination for three of these critical loadings: (1) the loading used for measurements on the divided shield, (2) a slightly different loading used for comparison measurements in open water, and (3) the loading used to obtain data for the measurement of energy release per fission. Several experiments and calculations pertinent to the

---

* In Part I, ORNL-1027, the major title read: Determination of the Power of the Shield Testing Reactor. The term "Bulk Shielding Reactor" has been substituted for "Shield Testing Reactor" to avoid confusion with the Submarine Thermal Reactor, referred to as the STR.

(1) References are listed at the end of this report.

operation of the reactor are described in the appendices.

Critical Assemblies

A list of all the critical reactor assemblies used at the BSF to date is given in Appendix A. Power calibrations have been made for the following reactor loadings.

Loading No. 2

The first critical assembly for which a power determination was made was described in Part I. The lattice configuration for this reactor consisted of a 5 by 5 arrangement of the fuel elements which was surrounded by water on all sides except the rear where a beryllium oxide reflector was located. Figure A-2 in Appendix A (Fig. 1 in Part I) shows this lattice configuration.

When this reactor was in place against the unit shield mockup,[2] there was only about an inch of water between the front row of fuel elements and the borated water of the shield. This so altered the thermal flux patterns within the reactor, particularly in the north (front) row, that a new power determination was made for these experiments.[3]

Loading No. 8

For the experiments on the divided shield mockup,[4] it was decided to construct a beryllium oxide--reflected reactor which would completely fill the assembly grid and thus present a surface as large as possible to the shield. The critical configuration which met this criterion is shown in Fig. A-4 in Appendix A. In addition to the permanent beryllium oxide

reflector at the back, reflector elements were also placed on the other three vertical sides.

The top and bottom of the lattice, of course, remained water-reflected. The active lattice was a 7 by 4 array of fuel elements with the back (south) row only partially filled with fuel. It should be noted that a partial fuel element was placed in the center of the south row and that the two reflector elements were placed in positions adjacent to the fuel elements in the ends of this row. For purposes of comparison, shielding measurements were required not only behind a shield sample (see below) but also in the water without the shield in place. The latter measurements are commonly referred to as experiments with the reactor in "open water." For the divided shield experiments, the fuel assembly arrangement used in open water is shown in Fig. A-4 of Appendix A. The data for this configuration appears in Appendix B and is referred to as Experiment 6. The critical mass of this arrangement was slightly less than 3.1 kg.

Loading No. 9

The divided shield mockup, Fig. 1, was a tank-like structure filled with borated water. Figure 2 shows a plan view of the reactor in the shield. It is to be noted that the shield extends not only in front (north) of the reactor, but also on both the east and west sides. It was found that the presence of the boron in the shield affected the power of the reactor in spite of the 3-in. beryllium oxide reflector between the active lattice and the shield. Not only was the power altered, but the loading of the back (south) row (see Fig. A-6 in Appendix A) had to be changed when the reactor

was in the shield. A full fuel element was placed in the center of this row, flanked by the beryllium oxide-reflector pieces which had been adjacent to the corner fuel elements in the open water reactor.

The flux patterns in the two reactors (Loadings 8 and 9) were quite different, not only owing to the modified loading, but also to the presence of the shield on three sides of one reactor. This necessitated complete mapping of the thermal-neutron flux distribution in each configuration. The data on this configuration appears in Appendix B as Experiment 7. The critical mass of this reactor was 3.1 kg.

Loading No. 11

Although no separate power determination was made on this critical assembly, it was used with the reactor inside the divided shield (as in Fig. 2) for making gamma spectral measurements. The lattice was similar to Loading 8 (see Appendix A, Fig. A-4). However, instead of the borated water in the shield as for Experiment 7 (Loading 9), the shield was filled with plain water. The power of this reactor was interpolated as being intermediate between that of Experiment 6 (Loading 8) and that of Experiment 7 (Loading 9).

Loading No. 15

An experiment is being conducted in the Bulk Shielding Reactor for determining the energy release per fission. For this experiment, the lattice was arranged as shown in Fig. A-9. This configuration is usually referred to as the "offset reactor." The arrangement was desirable because it provided one lattice position (37) which was completely

surrounded by full fuel elements. Several experiments, in addition to the calibration, were performed with this loading: (1) complete mapping of the thermal flux in and around position 37, (2) measurement of fission rate in the uranium fuel using "catcher" foils, (3) thermocouple measurements of heat generated in and around position 37, and (4) measurement of O^{16} and O^{17} cross sections. Some of these experiments will be discussed in more detail below; others will appear in separate reports. The critical mass of this configuration was 2.4 kg and the thermal flux data appears in Appendix B as Experiment 11.

Thermal-Neutron Flux Measurements and Power Calculations

Thermal-neutron flux measurements were made throughout each of the reactors by the activation of gold foils. The method is described in detail in Part I. In mapping both of the divided shield reactors (Loadings 8 and 9 above, and Figs. A-4 and A-6), advantage was taken of symmetry around the north-south centerline of the reactor. The validity of this assumption has been demonstrated for the unit shield reactor,[3] and the measurements were not repeated in the divided shield configurations. However, no such symmetry existed for the "offset reactor" (Loading 15 above and Fig. A-9), and measurements were necessary throughout the entire lattice. The experimental data for each of these lattice configurations appear in Tables B-1, B-4, and B-7 of Appendix B.

Tables B-2, B-5, and B-8 in Appendix B contain the data for neutron traverses throughout each reactor. The method of plotting this data was the same as that used in Part I and therefore the curves are not included.

The only significant difference between the earlier and present power calibrations is that the present calibrations include very few interpolated points.

The power of each reactor was calculated following the method outlined in Part I. Since the thermal-neutron flux distribution throughout the reactor, the amount of uranium in the reactor, and the fission cross section are known, the fission rate could be calculated. An energy release of 165 Mev/fission was assumed as before to calculate the power. This procedure is described in detail in Part I. Tables B-3, B-6, and B-9 show the power calculations for each of the beryllium oxide--reflected reactors.

Measurements on the Special Element

A special fuel element was constructed for the Mev/fission experiment (Fig. 3). It was similar to the usual elements with respect to the number of fuel plates and their spacing, the total amount of uranium, and the dimensions of the active part of the element. However, there were important differences. The ends of the box were designed to take water tubes, so that the water flow through the element could be measured and controlled, and thermocouples for measuring the water temperature were added at several points inside the element[5] (see Fig. 3). The center fuel plate was removable. This plate had nine discs 1-1/4 in. in diameter punched almost out along its vertical centerline, their centers being on the median plane and at 3, 6, 9, and 10-1/2 in. above and below the median plane (see Fig. 3). When desired, any of these discs could be removed and replaced either by another solid disc or by a disc-shaped "sandwich" made of three pieces: a core of the usual uranium-aluminum alloy, 20 mils thick, with a piece of

[redacted]

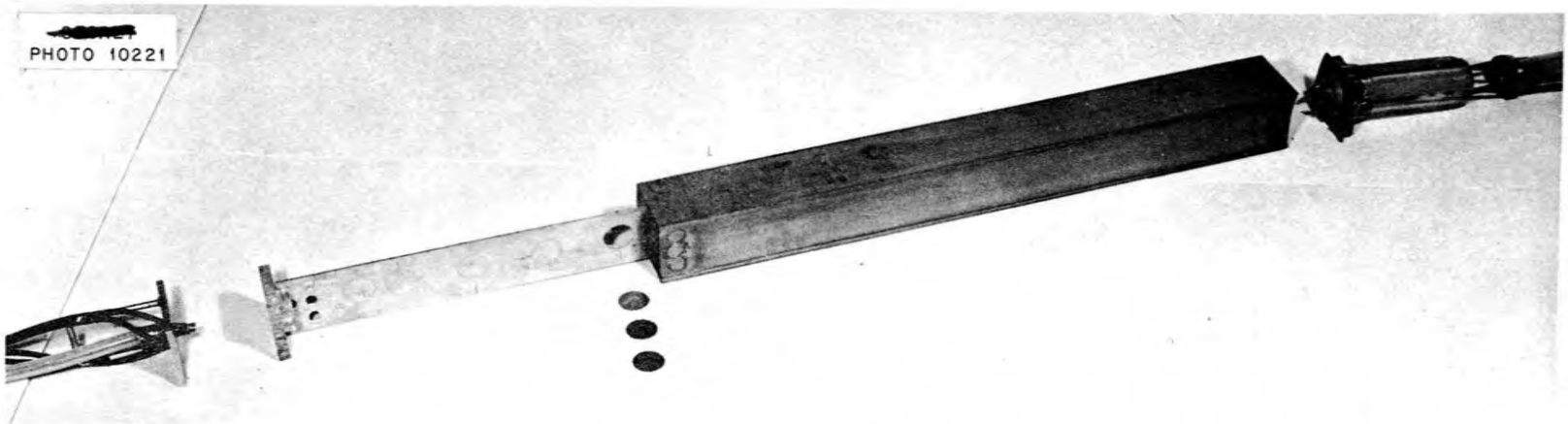

Fig. 3. Special Fuel Assembly. (Shows Center Fuel Plate, Removable Disks, Thermocouples and Water Tube.)

20-mil aluminum on each side. These outer pieces were the "catcher" foils used to measure the fission rate in the uranium.[5]

The thermal-neutron flux distribution in and around this special element was measured in much greater detail than is customary for a power calibration. Gold foils were placed at 3-in. intervals in vertical traverses on all four sides of the special element and at the centers of the punchings on the center fuel plate. Also, to assist in leakage calculations, neutron traverses (foils at 6-in. intervals) were measured on the west and east sides, respectively, of the fuel elements in lattice positions 36 and 38, adjacent to the special element in position 37. For convenience, the thermal-neutron flux data pertinent to the special element is given in Table B-10 (Appendix B). Figures 4 and 5 show the flux patterns on the four sides and down the center of this element. A comparison of these curves and data show that the flux distribution across this element, while not as flat as had been hoped, shows no sharp breaks. Figure 6 shows the variation of the cadmium ratio with distance from centerline on the special element.

For a part of this experiment (the thermocouple runs), it was necessary to clad the outside of the element with grease for thermal insulation. In addition, grease was used as a water seal over the "catcher" (fission) foils when they replaced the punchings in the center fuel plate. Gold foil measurements were made on the adjacent faces of surrounding elements to determine whether the presence of the grease altered the neutron flux in the vicinity. It was concluded from these measurements that, if any difference did exist, it was well within the statistical errors in foil counting.

[redacted]

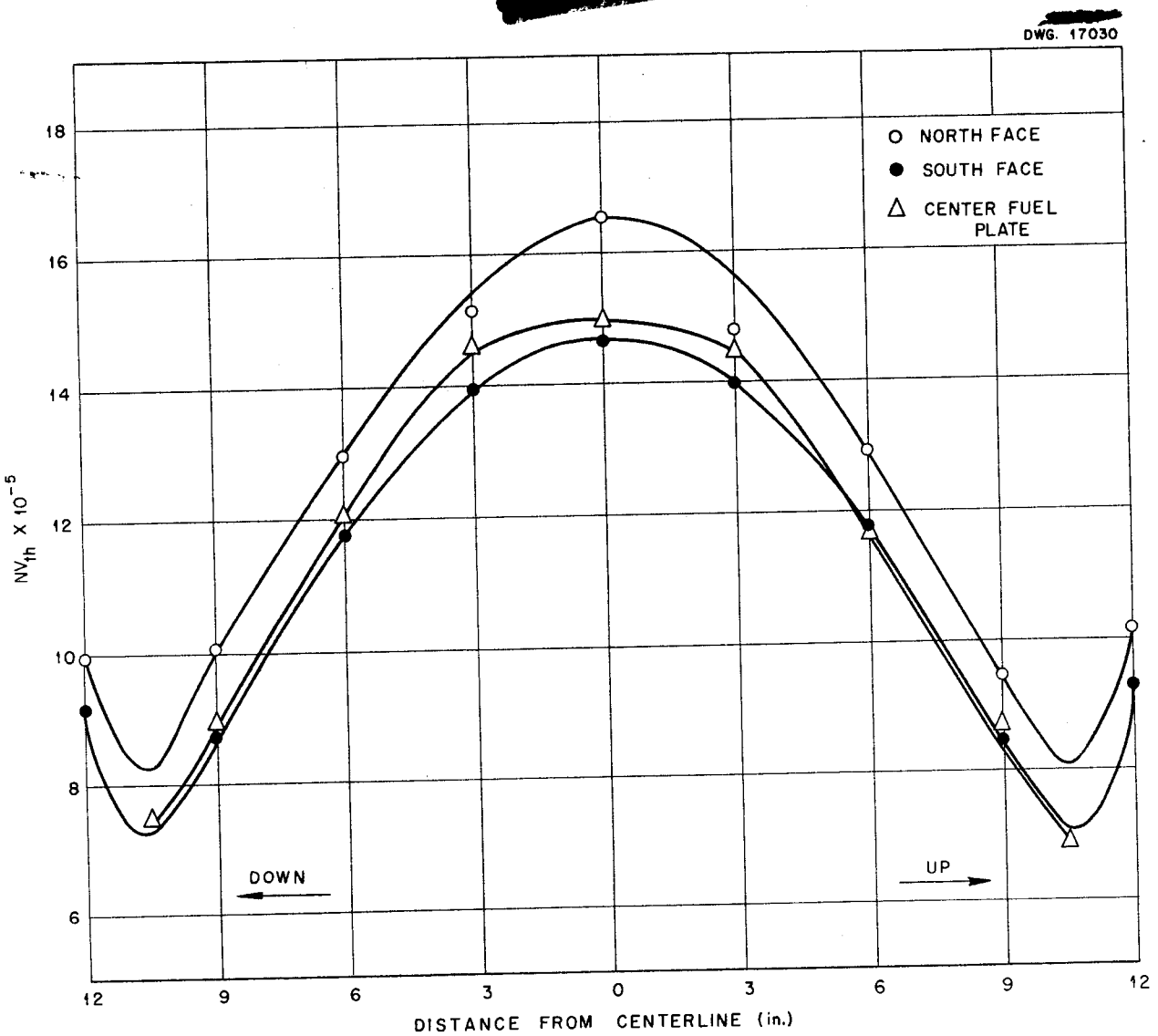

Fig. 4. Thermal-Neutron Flux Distribution on the Special Fuel Element (Vertical Traverses).

[redacted]

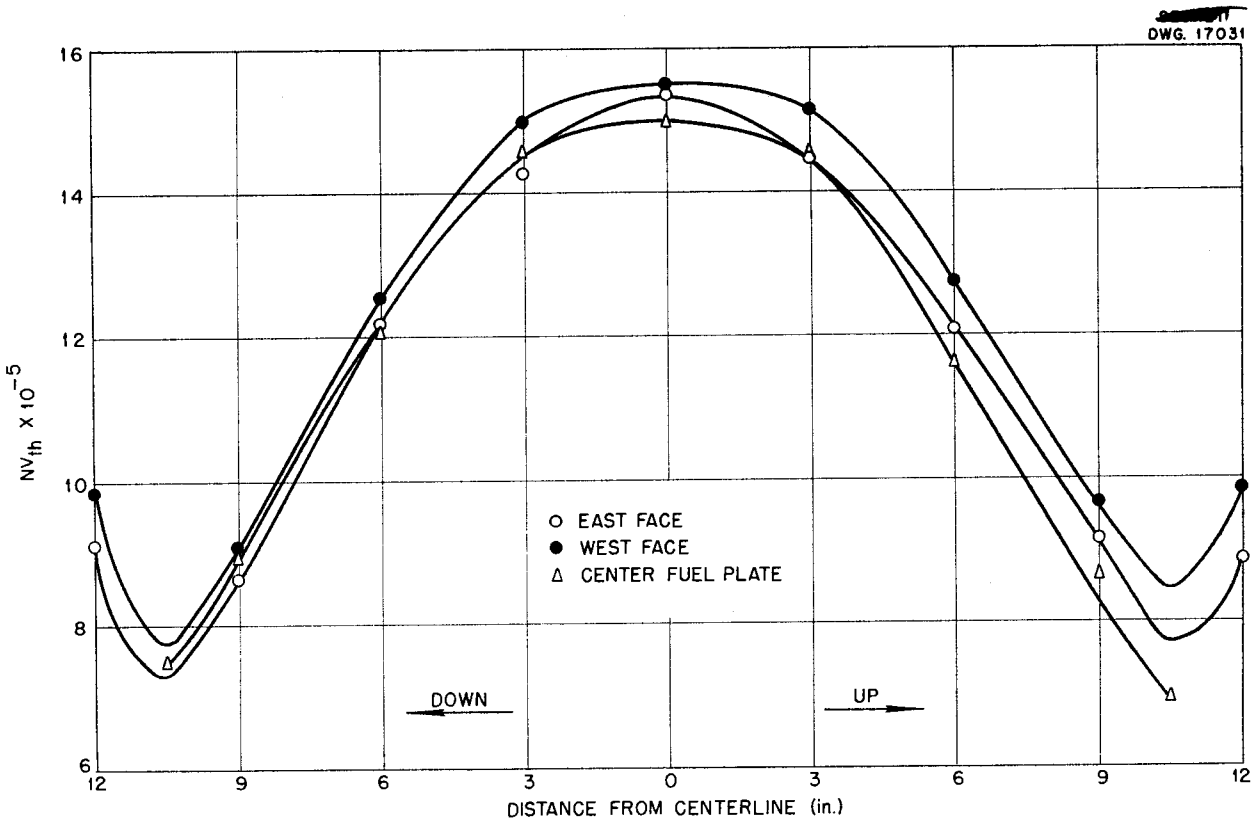

Fig. 5 Thermal-Neutron Flux Distribution on Special Fuel Element (Vertical Traverses).

[redacted]

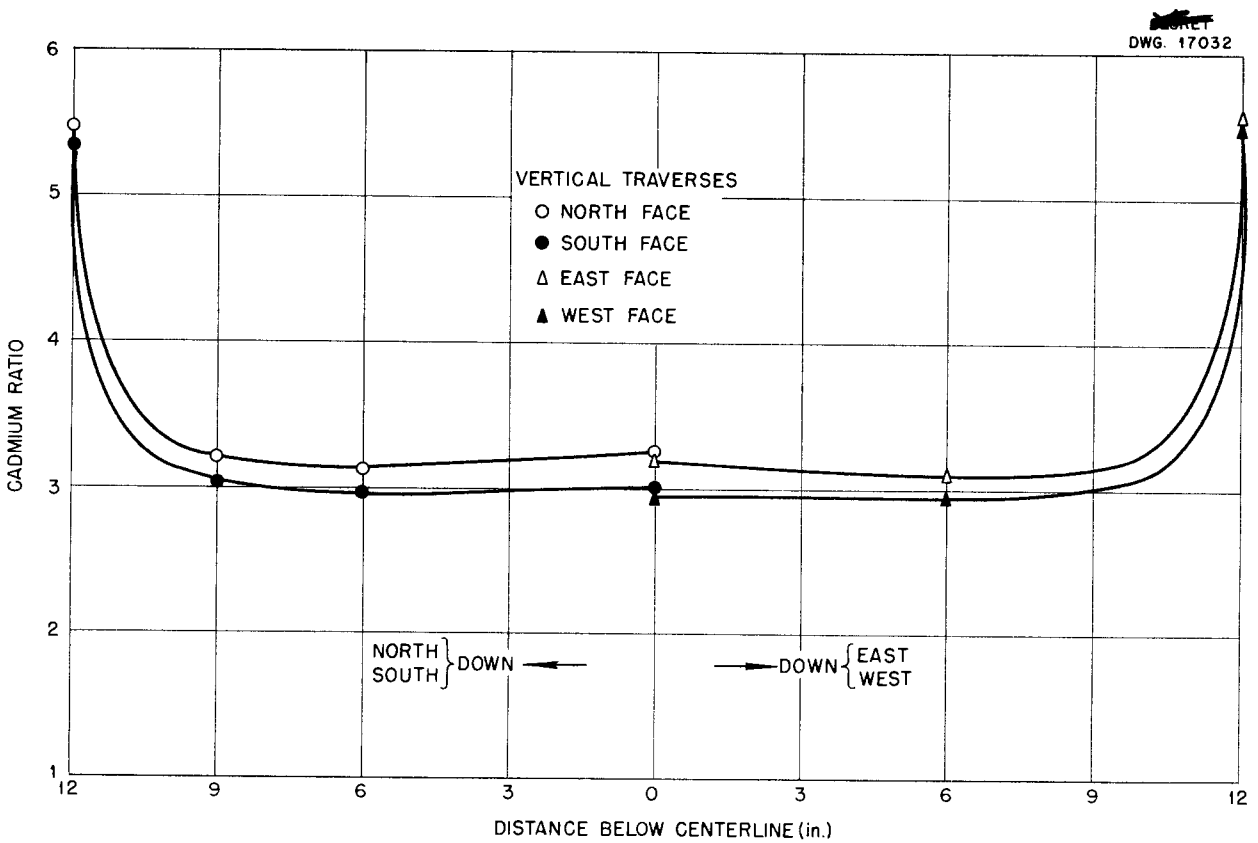

Fig. 6. Variation of Cadmium Ratio with Distance from Centerline on the Special Fuel Element.

Results

The reactor is operated at a power level of one nominal watt or some known multiple thereof. This nominal watt power level is set for the reactor instruments on the basis of the activity induced in gold foils exposed in the reactor prior to a complete calibration. After the reactor has been calibrated so that the actual power is known, all measurements made with a particular lattice configuration are "normalized" to the actual power of the reactor.

The total power of the divided shield reactor in open water was 0.991 watts/nominal watt (Table B-3, Appendix B); of the divided shield reactor in the shield, 0.853 watts/nominal watt (Table B-6); and of the "offset reactor," 1.054 watts/nominal watt (Table B-9). All measurements made in the latter critical assembly were "normalized" to a power level of 1/10 nominal watt. Since this was the power at which the fission foils were activated (see Ref. 5), it was felt that results would be easier to interpret if the data from the gold foil runs were normalized to that from the fission foil runs rather than vice versa. For this reason Table B-9 shows a total reactor power of 0.1054 watts. Tables B-3, B-6, and B-9 show the power generated in each fuel element and in each row of fuel. Figures 7, 8, and 9 show the power distribution in each of these reactors.

Figure 10 is a comparison of the power distribution in the two divided shield reactors. It is interesting that the greatest differences in the two reactors occur exactly as expected, i.e., in the north (front) and south (back) rows. The power in the north row of the reactor in the

[redacted]

DWG. 17026

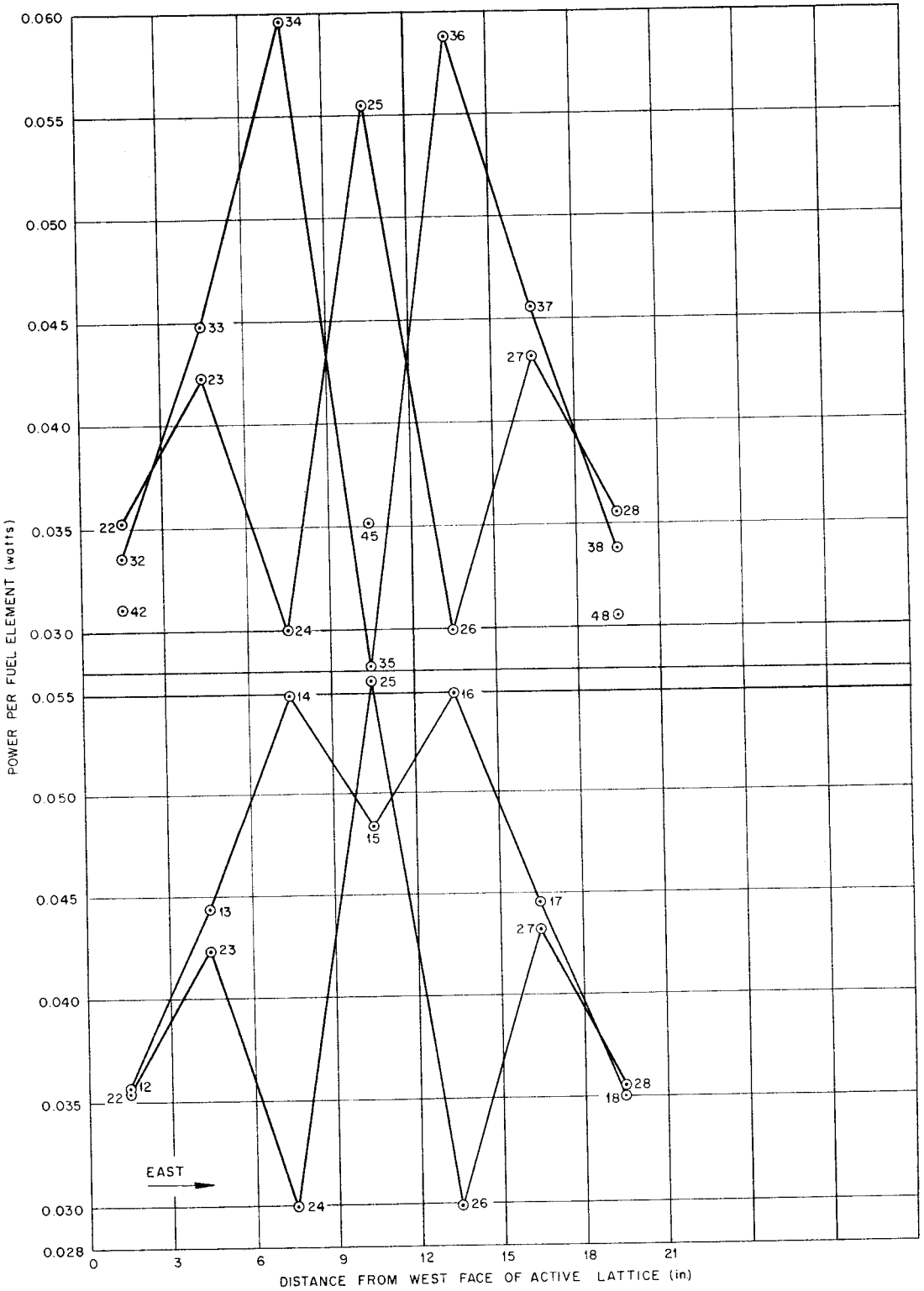

Fig. 7. Power Distribution in the Open Water Divided Shield Reactor (Experiment 6, Bulk Shielding Facility).

East-West Traverses by Rows

[redacted]

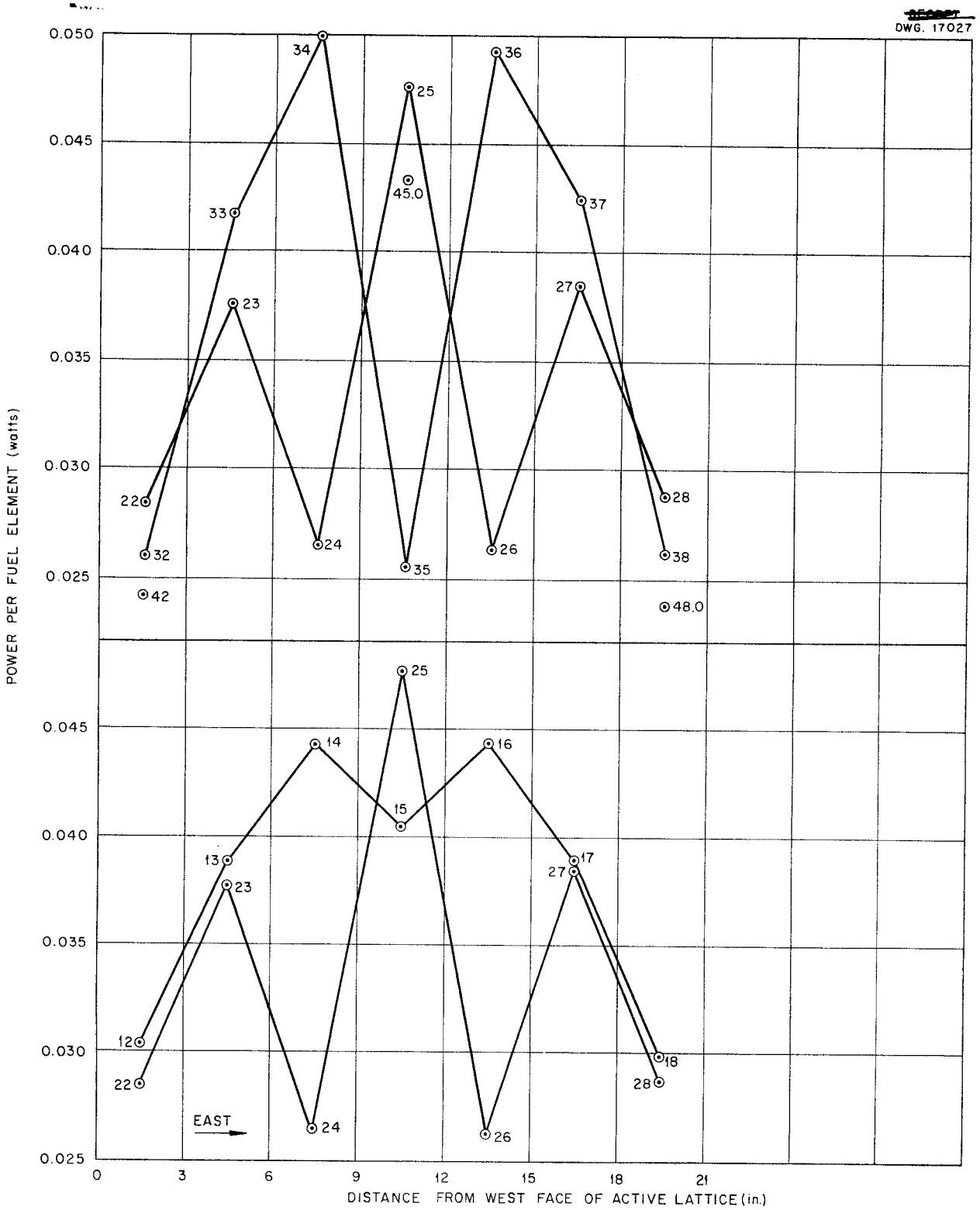

Fig. 8. Power Distribution in the Divided Shield Reactor (Experiment 7, Bulk Shielding Facility) East–West Traverses by Rows

[redacted]

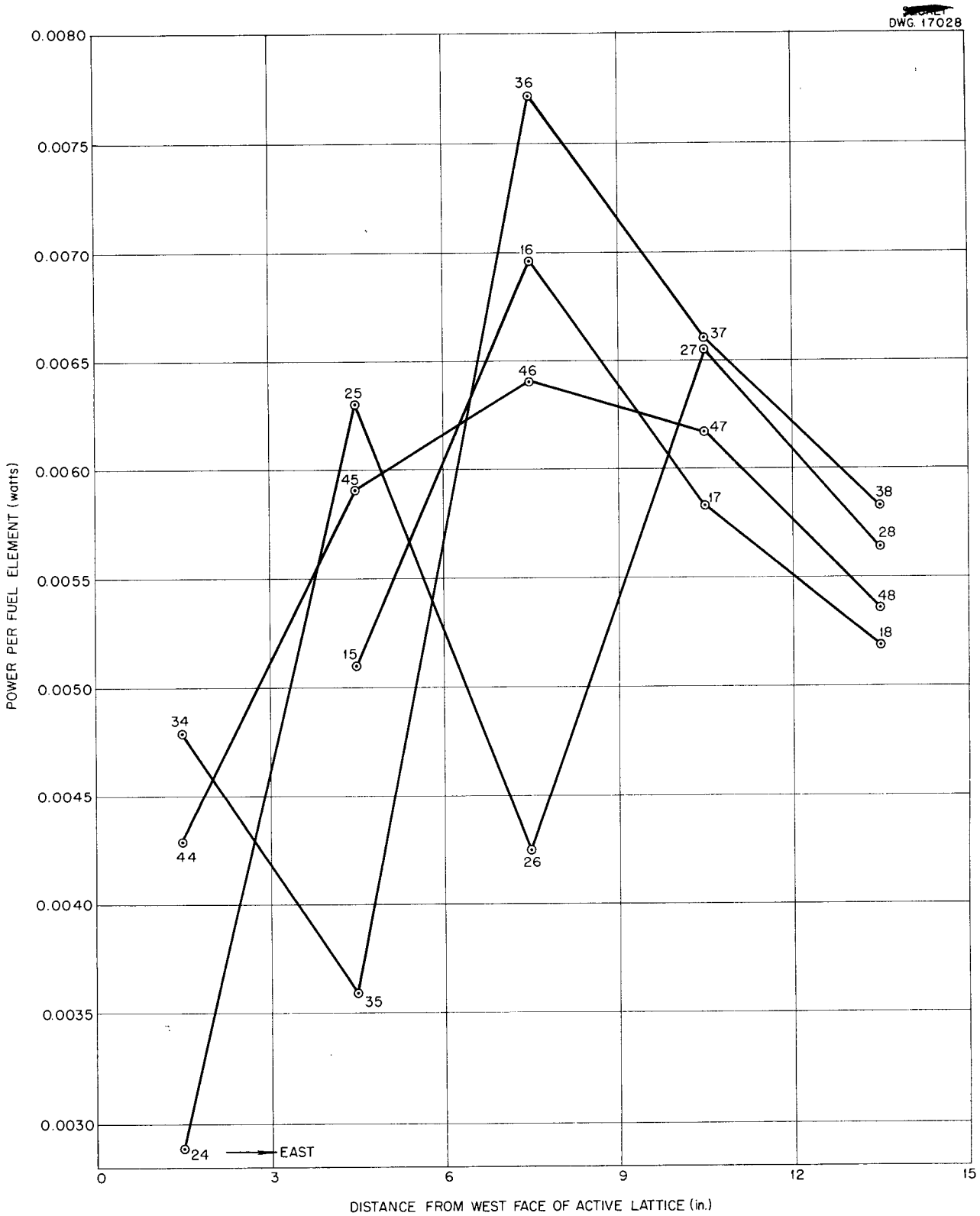

Fig. 9. Power Distribution in the "Offset Reactor" (Experiment 11, Bulk Shielding Facility). East-West Traverses by Rows

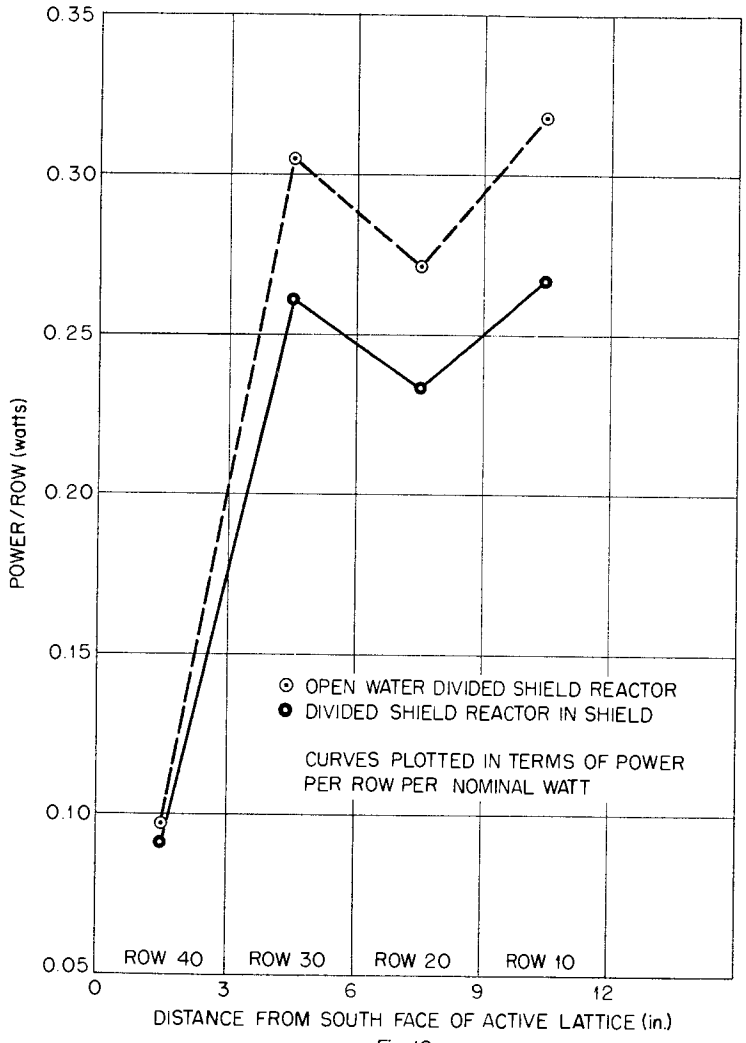

Fig. 10a

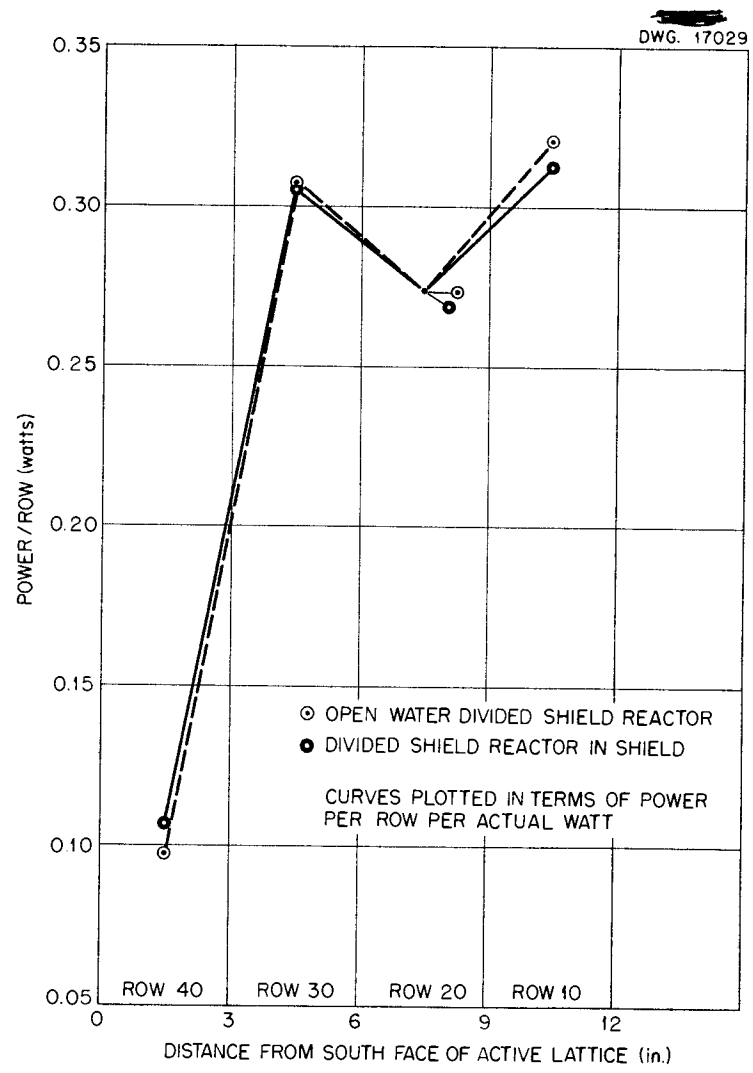

Fig. 10b

Comparison of Power Distributions Through the Bulk Shielding Reactors.

shield is slightly depressed owing to the presence of borated water in the adjacent shield, while the south row shows higher power than it did with the reactor in open water owing to the full fuel element in the center of the row and the location of the beryllium oxide--reflector pieces (see Critical Assemblies, Loadings 8 and 9 above; see also Figs. A-4 and A-6, Appendix A). Figure 10b is a comparison of the power distribution in the two reactors, plotted in terms of power per row per unit total actual power.

It should be pointed out that Figs. 7, 8, 9, and 10a are plotted in terms of observed values, i.e., although the two reactors compared in Fig. 10a showed quite different actual total power, the points shown on these curves are with reference to the "nominal" power as indicated by the reactor control instruments.

Figure 11 shows a comparison of the thermal-neutron flux distribution along the north-south centerline of both the unit shield and divided shield reactors in open water. The curves are extended to show the attenuation in the water along the centerline. Table B-11 is a collection of the pertinent data from several sources. It will be noted that the thermal flux at the north face is considerably higher in the case of the beryllium oxide--reflected divided shield reactor than for the water-reflected unit shield reactor and that the relaxation length of the thermal neutrons leaving the reactor is shorter in about the nearest 20 cm of water. Leakage calculations (Appendix C) show that the leakage from the north face of the 7 by 4 beryllium oxide--reflected reactor in open water was about 36% higher than for the 5 by 5 water-reflected reactor.

[redacted]

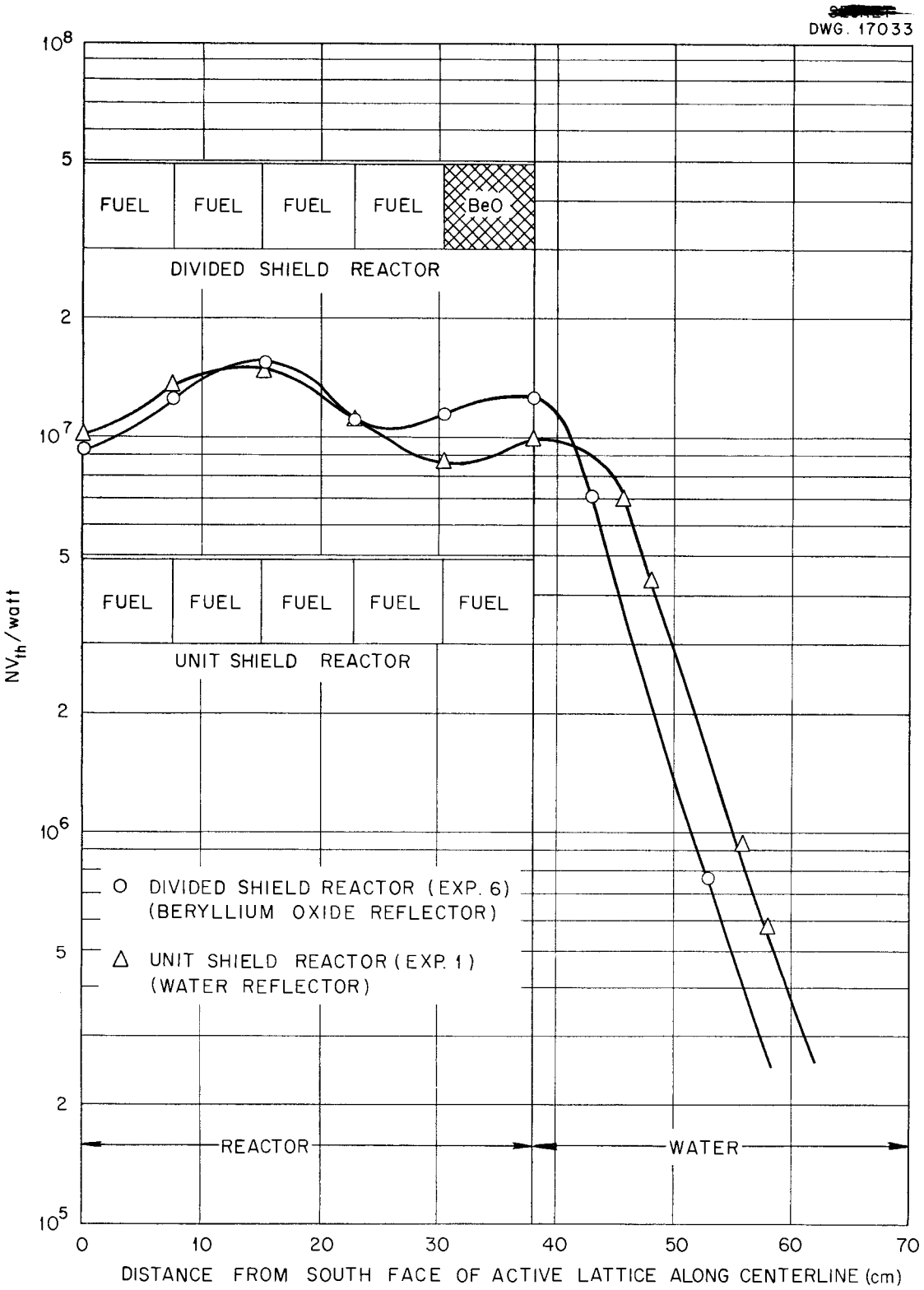

Fig. 11. Comparison of Thermal-Neutron Flux Distributions in the Unit Shield and Divided Shield Reactors; Bulk Shielding Facility. North-South Traverse along Centerline.

Discussion of Errors

It is felt that the total effect of all errors in actual foil exposures and counting, including determination of the thermal-neutron flux distribution, is certainly not greater than 5% and probably closer to 2%, assuming correct calibration of the Standard Pile (see below). Individual determinations may be in error by as much as 10%, particularly the measurements made 12 in. from the centerline, since these foils are half on and half off fuel and very slight deviations in positioning will be magnified in the observed activity (see Appendix E).

Since the completion of the present determinations, the results of the recalibration of the Standard Graphite Pile have become available.[6] Klema reports a thermal flux of 703 neutrons/cm^2/sec in slot 11, which is to be compared with the previous value of 654 neutrons/cm^2/sec in the same position. This, of course, means that all thermal flux values determined on the basis of the old calibration must be increased by a factor corresponding to the above results (see Appendices D and E for details of the procedure). However, all data taken to date are reported on the basis of the old Standard Pile calibration given in CP-2804[7] for ease of comparison with the data from the unit shield experiments. Should it be desirable to express the thermal flux values (and thus the reactor power) in terms of the recent Standard Pile calibration, the conversion can be made by multiplying the appropriate values by the ratio of the "nv_{th} factors," $\frac{3.29}{2.95} = 1.115$ (see Appendix E).

Two other probable sources of error in a power determination are as yet unresolved. A value of 165 Mev per fission as the energy release has been used in all power calculations, although this number is the subject of considerable controversy. An independent measurement of the energy release is being made at this facility[5] by forcing water at a known velocity through the special fuel element and measuring the temperature in several places in the fuel element. This data, together with that from the fission foils[5] which will establish independently the fission rate, should lead to a more accurate evaluation of the energy release.

It will be recalled that the thermal-neutron flux values as measured with foils depend on the "calibration" of these foils in the Standard Graphite Pile. This in itself introduces an uncertainty in that the foils are calibrated in a graphite medium and then are used to determine an unknown flux in a nonhomogeneous mixture of water, fuel, and aluminum in the reactor. Since the diffusion coefficients of the media are quite different, there is no reason to suppose that the presence of the foil would produce the same perturbation of the flux in each case. A semiempirical evaluation of the flux perturbation due to a 25-cm^2 indium foil exposed in a water medium but "calibrated" in a graphite medium has been made,[8] but no such correction has been made for gold foils. It is hoped that a comparison of the data from the fission foils and from the gold foils activated in the same positions in the special element will yield an effective evaluation of the flux perturbation due to the 1-cm^2 gold foils exposed in the reactor.

The net effect of the uncertainties still involved in a power determination by this method is difficult to evaluate accurately at this time. However, it is evident that both the effect of the recalibration of the Standard Pile and the effect of the difference in flux perturbation by a foil in graphite and in the reactor will increase the value of the thermal-neutron flux observed in the reactor, possibly as much as 30 to 40%. Obviously, the actual reactor power would be increased by the same amount. Preliminary results from the experiment using fission foils[6] indicate that the flux (based on Klema's recalibration of the Standard Pile) is in error by no more than 5 or 10%. A final evaluation must await the results of that experiment.

Acknowledgements

The authors wish to express their appreciation to Messrs. L. B. Holland and J. K. Leslie for their assistance in operating the reactor, and to Miss Grace McCammon for her assistance in counting the foils. Thanks are due Dr. E. D. Klema and Mr. R. H. Ritchie for their valuable suggestions concerning the Standard Pile calibrations.

Appendix A

LIST OF CRITICAL ASSEMBLIES

J. K. Leslie

This appendix includes diagrams of principle loading configurations only. Special loadings that were used only once or twice for irradiation of sources, etc., are described with reference to diagrams of principle loadings. Critical masses are given for each loading to the nearest 0.1 kg.

Loading No. 1 (2.4 kg) is shown in Fig. A-1. This was the first critical loading of the Bulk Shielding Reactor.

Loading No. 2 (3.2 kg) is shown in Fig. A-2. This critical experiment gave the mass necessary for criticality with the beryllium oxide reflector on the rear only.

Loading No. 3 (2.4 kg) is shown in Fig. A-3. The effect of rod position in the reactor was studied. The critical mass was almost identical with loading No. 1.

Loading No. 4 (3.2 kg) was the same as loading No. 2, but thermocouples and water tubes were added for a preliminary energy per fission experiment.

Loading No. 5 (3.1 kg) was the same as loading No. 2 except that a fuel element was replaced by a reflector element in position 43. A bismuth slab was used at the face of the reactor.

Loading No. 6 (3.1 kg) was the same as loading No. 2 except that reflector elements were added in positions 2, 12, 22, 32, 8, 18, 28,

[redacted]

[redacted]
DWG. 10527A

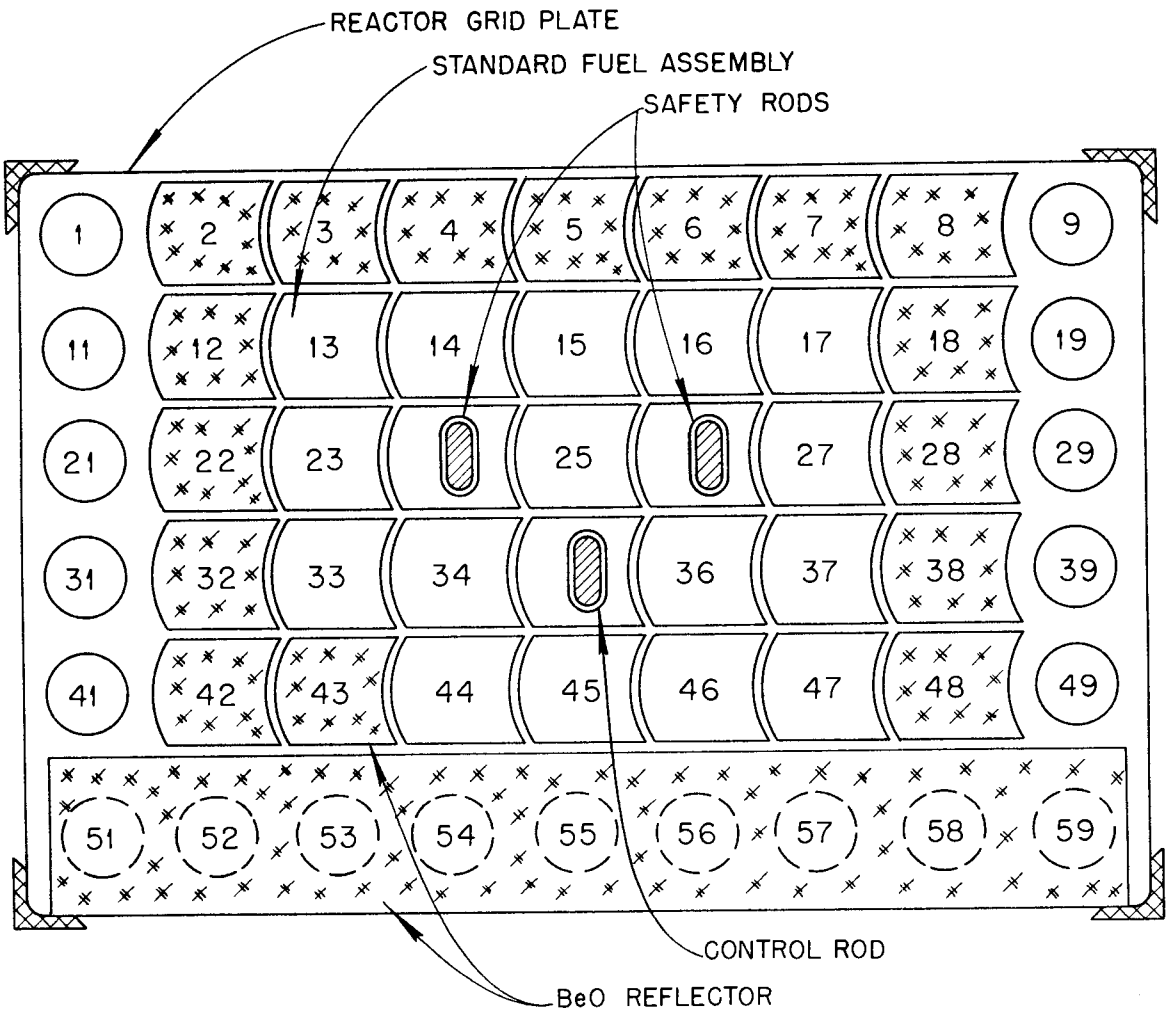

Fig. A-1. Fuel Assembly Arrangement – Critical Loading No. 1 of Bulk Shielding Reactor

[redacted]

~~SECRET~~
DWG. 10528A

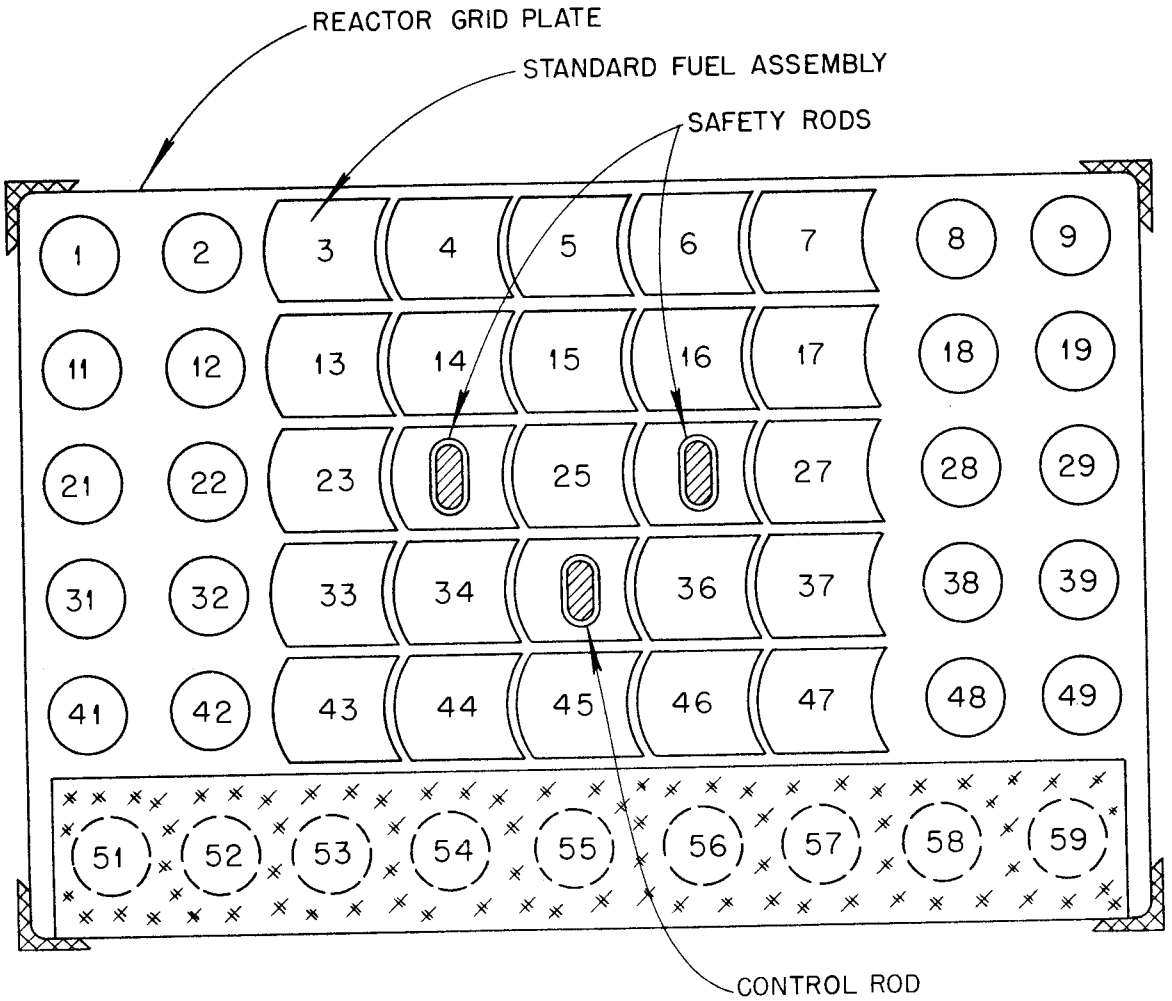

NOTE: BeO REFLECTOR ONE SIDE
WATER REFLECTOR THREE SIDES

Fig. A-2. Fuel Assembly Arrangement–Critical Loading No. 2 of Bulk Shielding Reactor.

[redacted]

[redacted]
DWG. 10529A

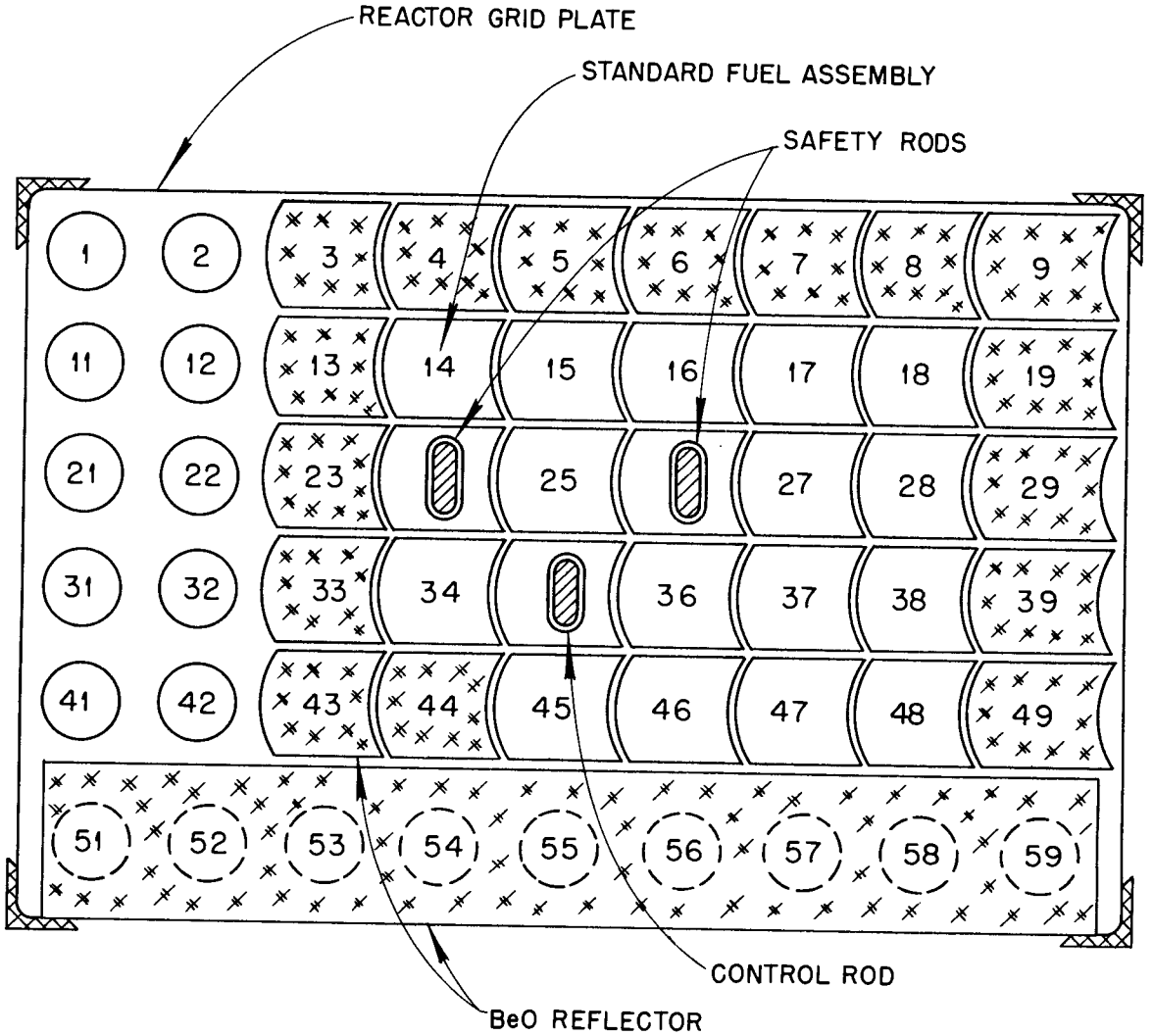

Fig. A-3. Fuel Assembly Arrangement-Critical Loading No.3 of Bulk Shielding Reactor.

and 38, and a fuel element was removed from position 15. A capsule of $NaNO_3$ was activated in position 15 to produce Na^{24}.

Loading No. 7 (3.2 kg) was the same as loading No. 2. This loading was also used for preliminary energy per fission experiments. Different fuel elements were used, but the critical mass was the same.

Loading No. 8 (3.1 kg) is shown in Fig. A-4 and was the open water loading similar to the divided shield loading, as described in the body of this report.

Loading No. 8B (3.1 kg) is shown in Fig. A-5 and was the open water loading replacing loading No. 8. This change was made necessary when the 4 in. thick one-piece reflector in the back row was replaced with individual 3 in. thick reflector elements.

Loading No. 9 (3.1 kg) is shown in Fig. A-6 and was the divided shield loading similar to loading No. 8, as described in the body of this report.

Loading No. 9D (3.0 kg) is shown in Fig. A-7 and was the divided shield loading replacing loading No. 9. This change was made necessary when the 4 in. thick one-piece reflector in the back row was replaced with individual 3 in. thick reflector elements.

Loading No. 10 (3.1 kg) was the same as loading No. 8 except that position 41 was empty. This loading was used in a lead and concrete block temporary instrument shield.

Loading No. 11 (3.1 kg) was the same as loading No. 8 except that reflector elements were placed in positions 43 and 47, and positions 44 and 46 were empty. This was the divided shield reactor when the shield was filled with pure water (see the body of this report).

[redacted]

[redacted]

SSD-A-623
DWG. 17203

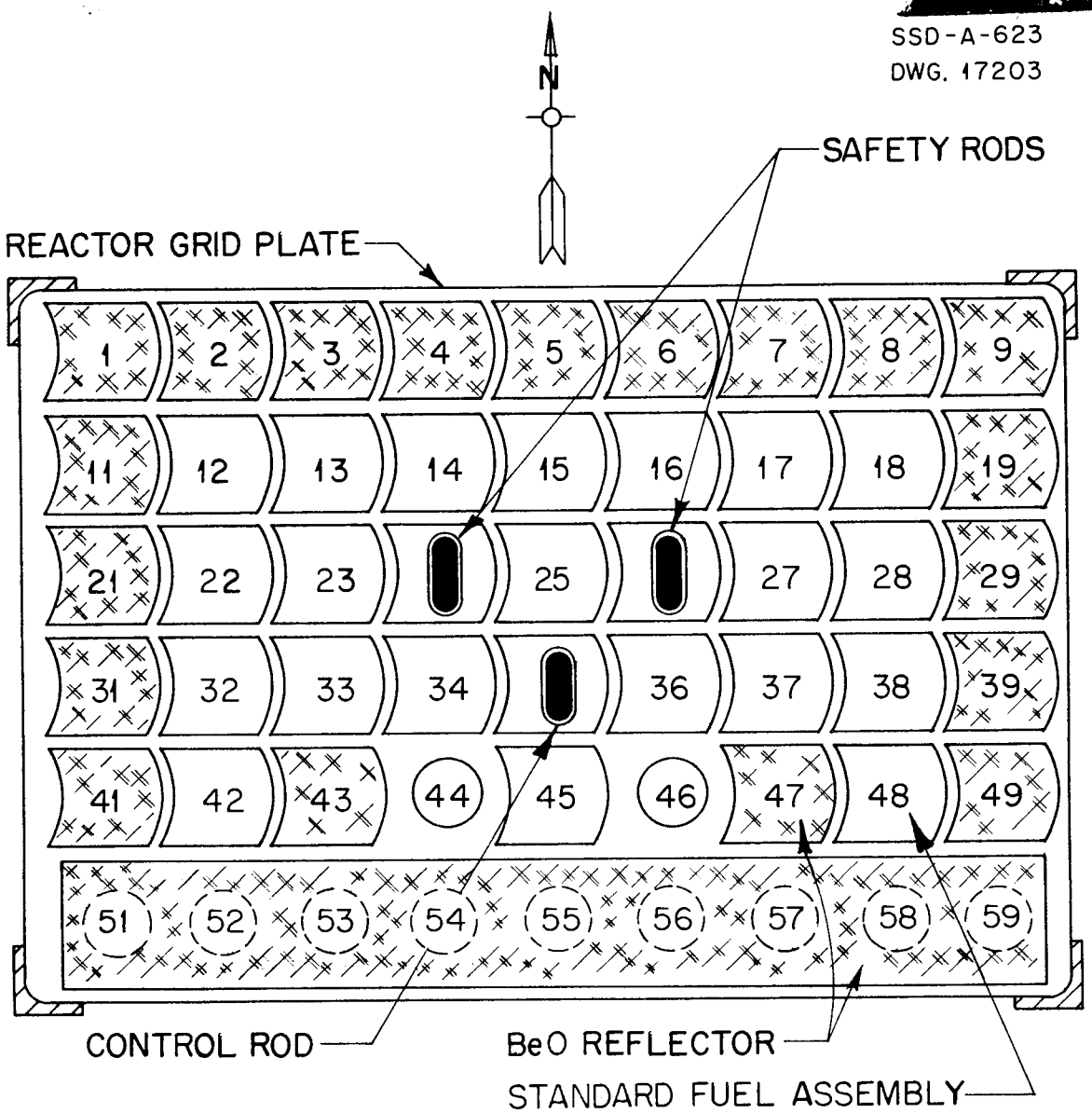

Fig. A-4. Fuel Assembly Arrangement - Critical Loading No. 8 of Bulk Shielding Reactor.

[redacted]

[redacted]

DWG. 17496

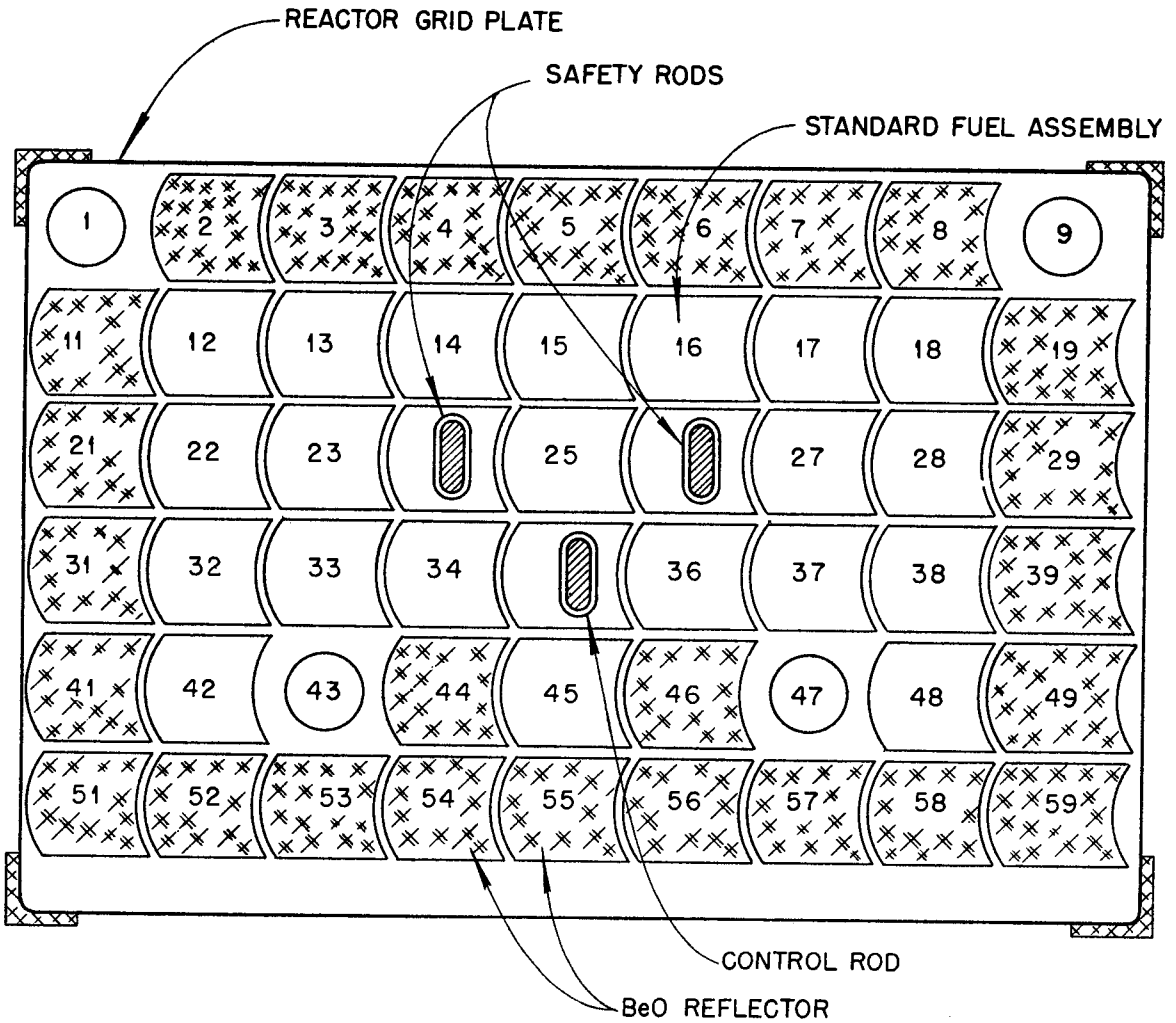

Fig. A-5. Fuel Assembly Arrangement - Critical Loading No. 8B of Bulk Shielding Reactor.

[redacted]

[redacted]

DWG. 14437A

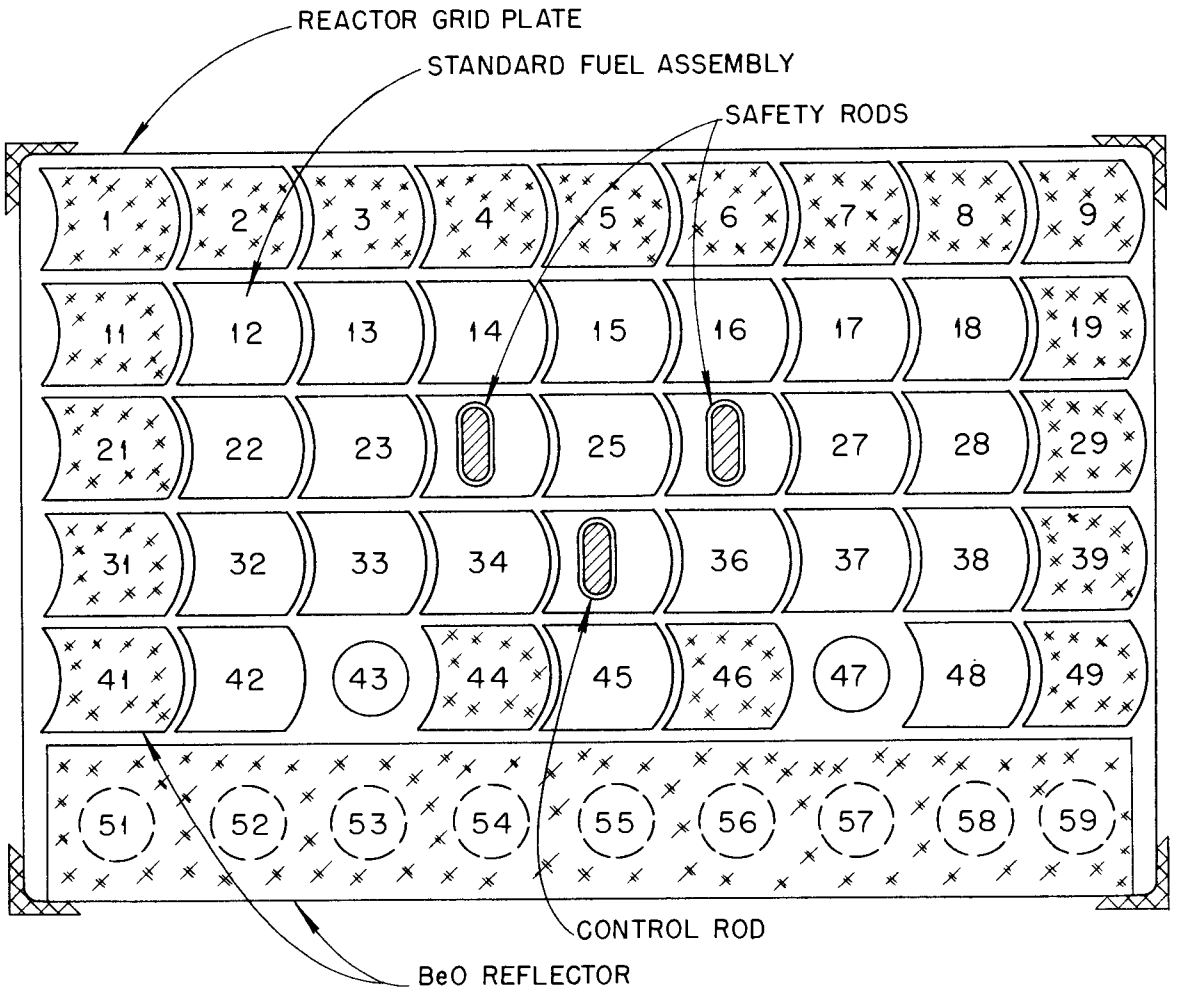

Fig. A-6. Fuel Assembly Arrangement – Critical Loading No. 9 of Bulk Shielding Reactor.

[redacted]

[redacted]

DWG. 17497

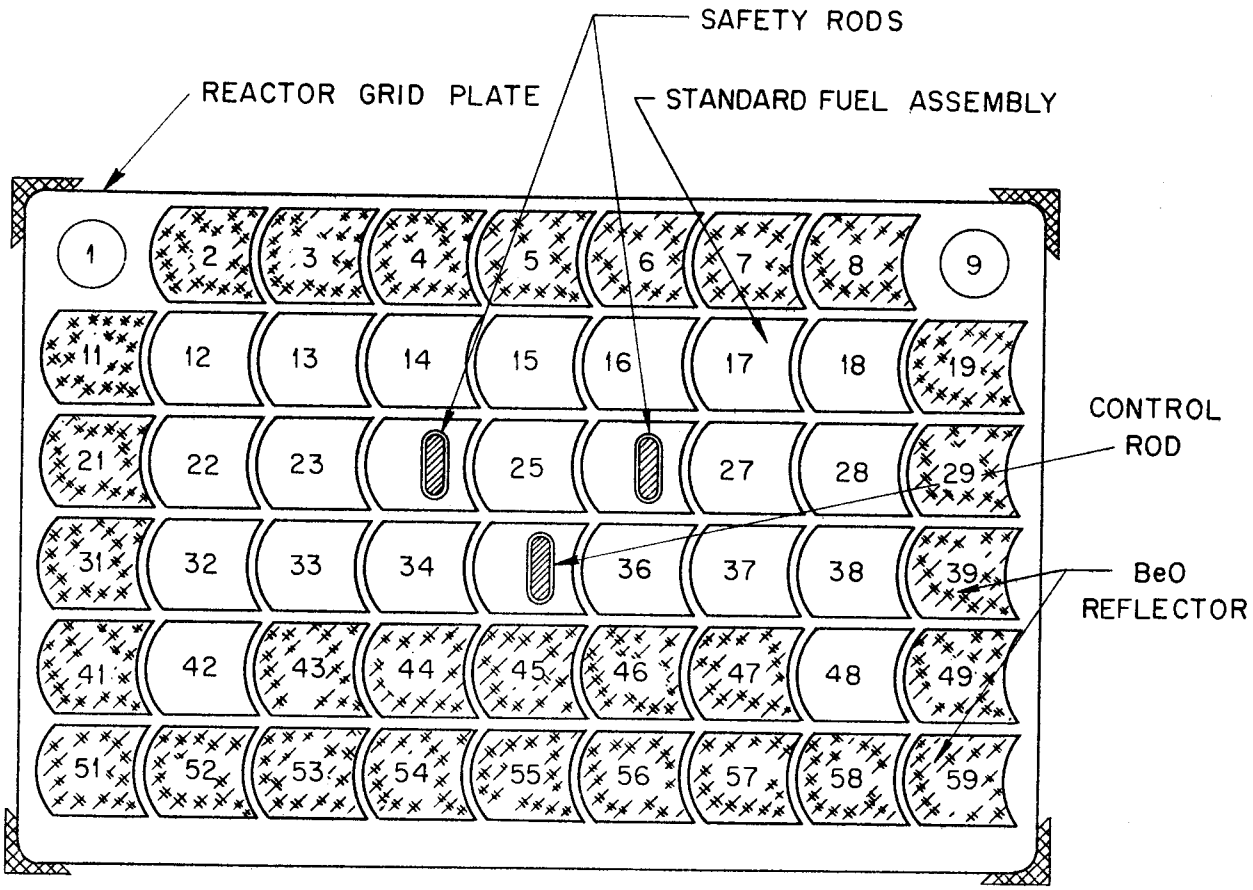

Fig. A-7 Fuel Assembly Arrangment - Critical Loading No. 9D of Bulk Shielding Reactor.

Loading No. 12 (3.1 kg) was the same as loading No. 8 except that a reflector element was added in position 46 and positions 5, 39, and 44 were empty. This loading was used for neutron spectrometer experiments.

Loading No. 13 (3.1 kg) was the same as loading No. 8 but with all cold elements. This loading was used for gamma spectrometer experiments.

Loading No. 14 (3.8 kg) is shown in Fig. A-8 and was used to test and calibrate stainless steel control rods.

Loading No. 15 (2.4 kg) is shown in Fig. A-9. This loading contained all cold fuel elements and was used for foil calibration of the power of the reactor to be used for energy per fission determination (see the body of this report).

Loading No. 16 (2.4 kg) was the same as loading No. 15 but with activated fuel elements.

Loading No. 17 (3.1 kg) is shown in Fig. A-10 and was used for threshold detector experiments.

Loading No. 18 (3.1 kg) was the same as loading No. 8B except that reflector elements were in positions 43 and 47 and positions 44 and 46 were empty. This loading was used for thermal column experiments.

Loading No. 19 (3.2 kg) is shown in Fig. A-11 and is being used for experiments now in progress on the mockup of the top plug of the Submarine Intermediate Reactor (SIR) shield. This loading is also being used for experiments with the thermal column. The measurements on the flux distribution have not been completed at this writing.

Loading No. 20 (3.3 kg) is the same as loading No. 19 except that a partial fuel element containing 70 g of U^{235} is substituted for the reflector element in position 45. This loading is used for long period operation at 100 kw and has sufficient excess fuel to override xenon buildup.

[redacted]

[redacted]

DWG. 17498

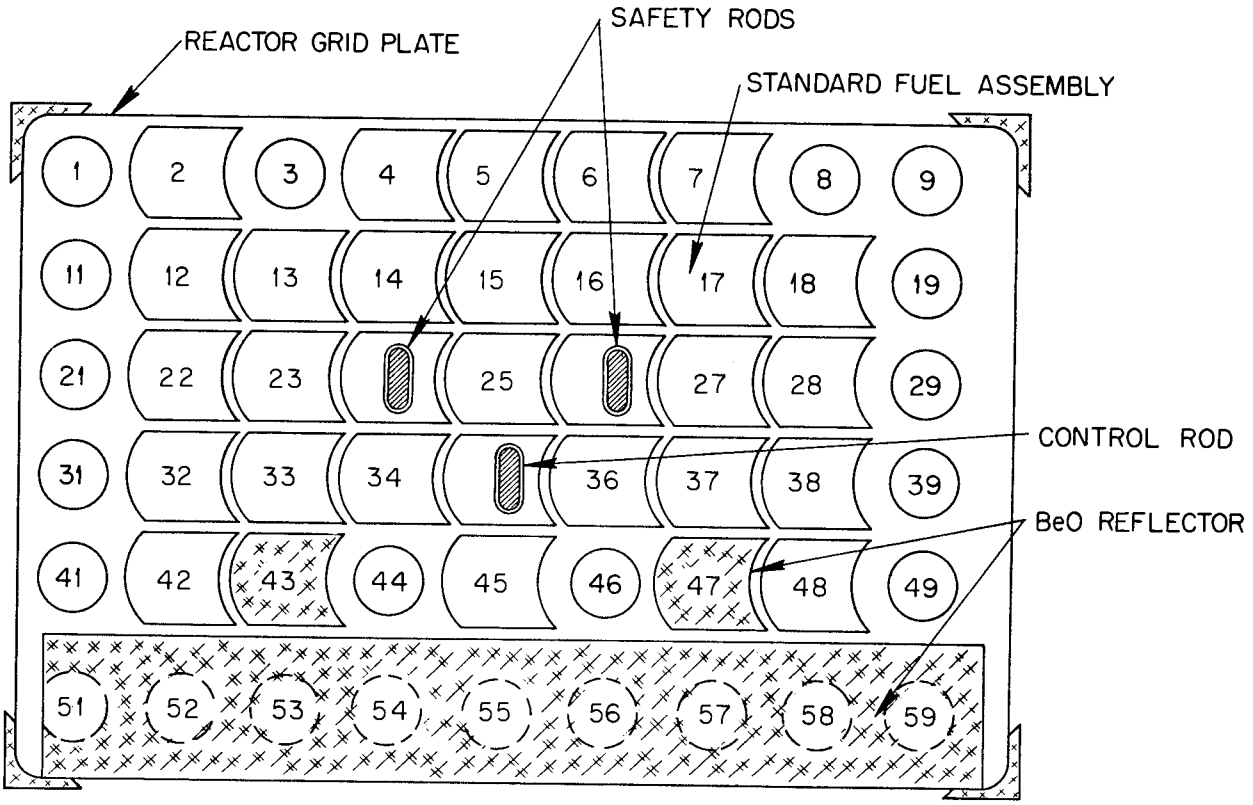

Fig. A-8. Fuel Assembly Arrangement - Critical Loading No. 14 of Bulk Shielding Reactor.

[redacted]

[redacted]

DWG. 17499

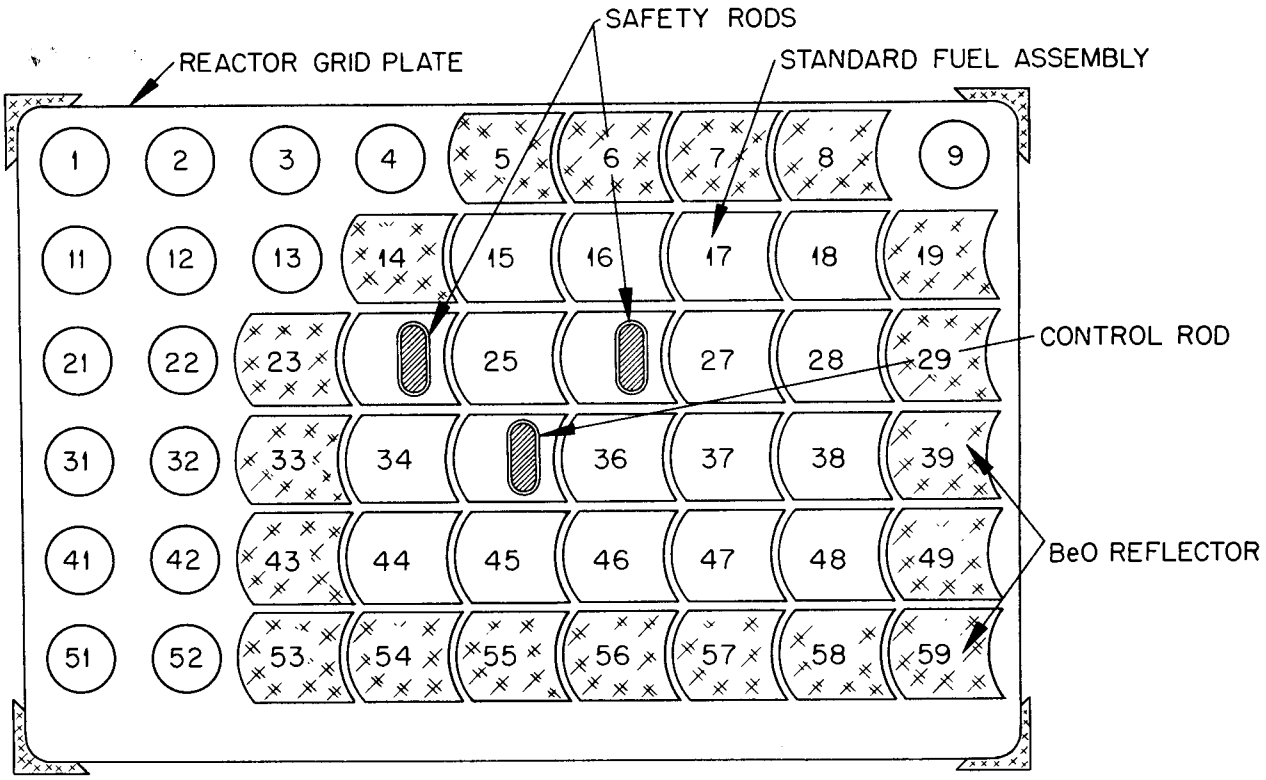

Fig. A-9. Fuel Assembly Arrangement — Critical Loading No. 15 of Bulk Shielding Reactor.

[redacted]

[redacted]

[redacted] WG.17202
SSD-A-622

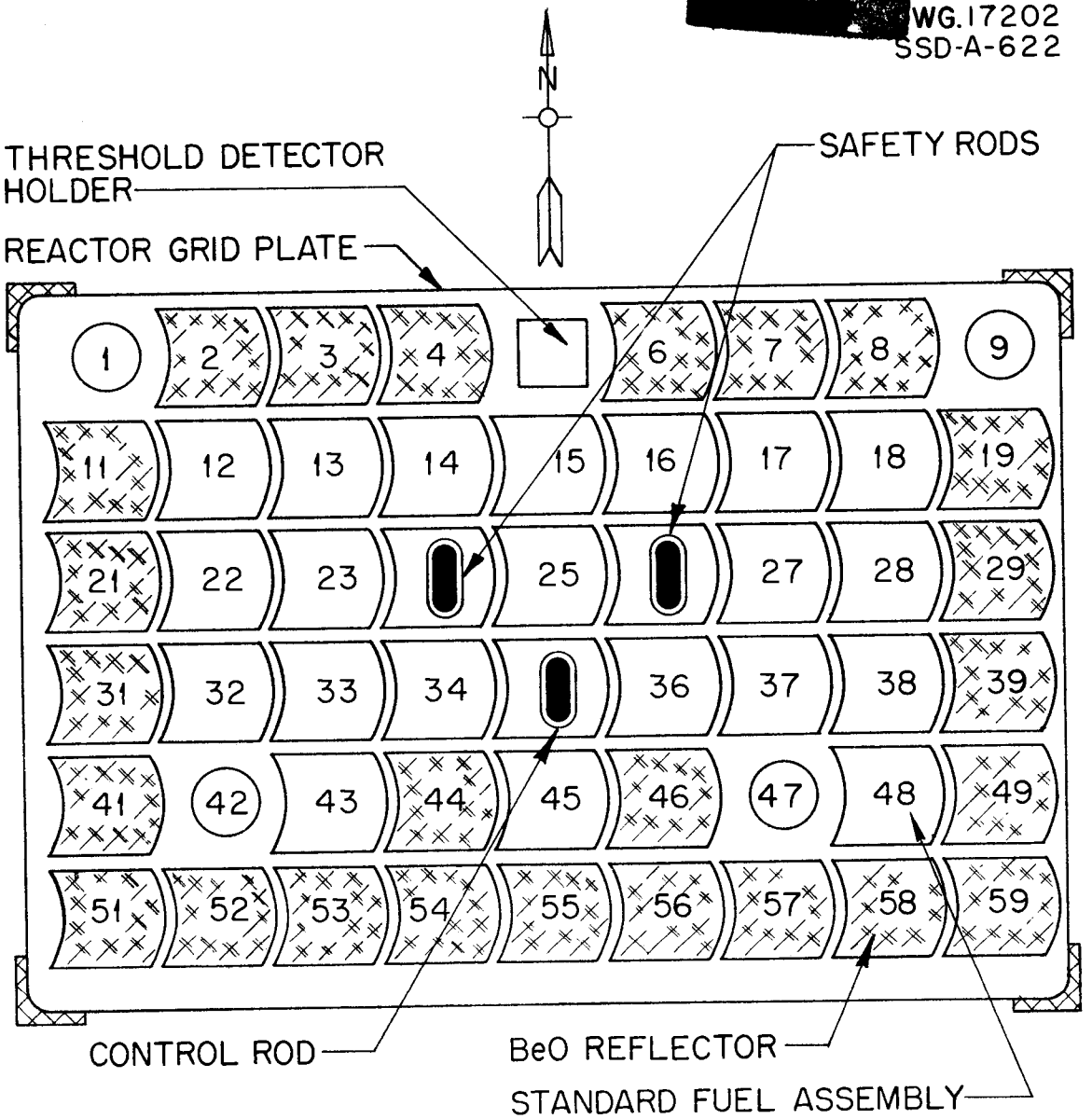

Fig. A-10. Fuel Assembly Arrangement - Critical Loading No. 17 of Bulk Shielding Reactor.

[redacted]

[redacted]
DWG. 18385

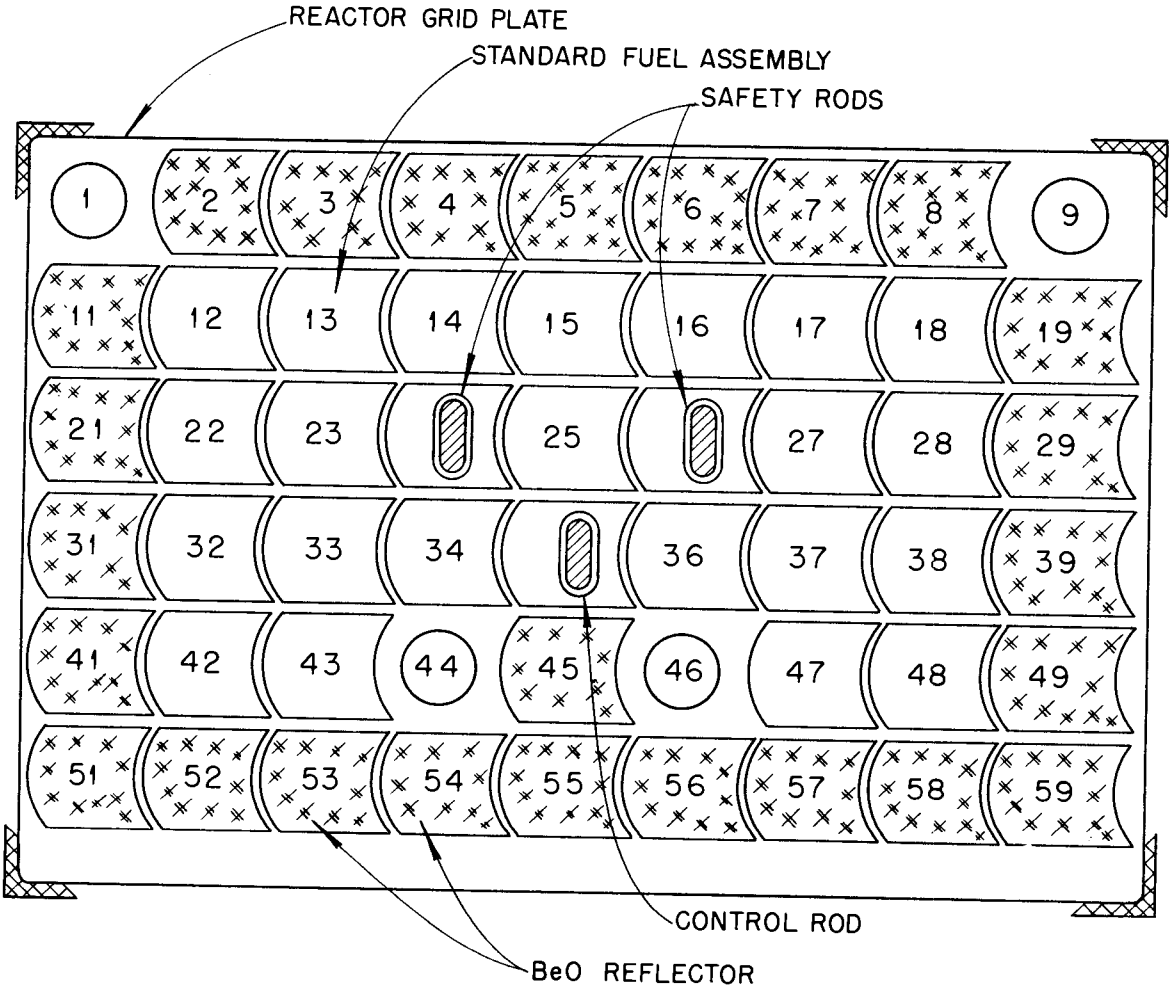

Fig. A-11. Fuel Assembly Arrangement - Critical Loading No. 19 of Bulk Shielding Reactor.

Appendix B

TABULAR DATA

This appendix contains all the data necessary for the power calculations for the three beryllium oxide--reflected reactors (Tables B-1 through B-9). Table B-10 is a summary of the thermal-neutron data taken on the special fuel element for the energy release per fission experiment. Table B-11 is a collection of data pertinent to a comparison of the thermal-neutron flux distributions along the centerline of both a water-reflected and a beryllium oxide--reflected reactor.

It should be noted that with the exception of Table B-10 all thermal-neutron fluxes are based on the Arnette and Jones calibration of the X-10 Standard Pile.[7]

Table B-1

Thermal-Neutron Flux Measurements in the Divided Shield Reactor (Experiment 6)

Lattice Position	Face	Position on Assembly	A_s Total	A_s Cd	A_s Thermal	Cd Ratio
15	North	℄	5.345×10^6	1.450×10^6	3.895×10^6	3.69
		6" above ℄	4.370×10^6			
		6" below ℄	4.422×10^6	1.200×10^6	3.222×10^6	3.68
		12"above ℄	2.579×10^6			
		12"below ℄	2.330×10^6	4.524×10^5	1.878×10^6	5.15
	South	℄	5.556×10^6	1.839×10^6	3.717×10^6	3.02
		6" above ℄	4.391×10^6			
		6" below ℄	4.395×10^6	1.505×10^6	2.890×10^6	2.92
		12"above ℄	2.904×10^6			
		12"below ℄	2.851×10^6	5.681×10^5	2.283×10^6	5.02
16	North	℄	5.307×10^6	1.399×10^6	3.908×10^6	3.79
		6" above ℄	4.340×10^6			
		6" below ℄	4.534×10^6			
		12"above ℄	2.528×10^6			
		12"below ℄	2.337×10^6	3.950×10^5	1.942×10^6	5.92
	South	℄	6.444×10^6	1.749×10^6	4.695×10^6	3.68
		6" above ℄	5.253×10^6			
		6" below ℄	5.280×10^6	1.440×10^6	3.840×10^6	3.67
		12"above ℄	2.957×10^6			
		12"below ℄	3.030×10^6	5.546×10^5	2.475×10^6	5.46

Table B-1 (continued)
(Experiment 6)

Lattice Position	Face	Position on Assembly	A_s Total	A_s Cd	A_s Thermal	Cd Ratio
17	North	℄	4.955×10^6	1.242×10^6	3.713×10^6	3.99
		6" above ℄	4.106×10^6			
		6" below ℄	4.072×10^6	1.029×10^6	3.043×10^6	3.96
		12"above ℄	2.353×10^6			
		12"below ℄	2.008×10^6	3.657×10^5	1.642×10^6	5.49
	South	℄	4.812×10^6	1.579×10^6	3.233×10^6	3.05
		6" above ℄	3.936×10^6			
		6" below ℄	3.968×10^6	1.278×10^6	2.690×10^6	3.10
		12"above ℄	2.600×10^6			
		12"below ℄	2.401×10^6	4.689×10^5	1.932×10^6	5.12
18	North	℄	3.623×10^6	8.984×10^5	2.725×10^6	4.03
		6" above ℄	2.916×10^6			
		6" below ℄	3.069×10^6	7.259×10^5	2.343×10^6	4.23
		12"above ℄	1.693×10^6			
		12"below ℄	1.640×10^6	2.762×10^5	1.364×10^6	5.94
	South	℄	3.963×10^6	1.246×10^6	2.717×10^6	3.18
		6" above ℄	3.171×10^6			
		6" below ℄	3.288×10^6	1.022×10^6	2.266×10^6	3.22
		12"above ℄	2.029×10^6			
		12"below ℄	2.038×10^6	3.254×10^5	1.713×10^6	6.26
25	South	℄	6.764×10^6	1.596×10^6	5.168×10^6	4.24
		6" above ℄	5.324×10^6			
		6" below ℄	5.499×10^6	1.360×10^6	4.139×10^6	4.04
		12"above ℄	2.539×10^6			
		12"below ℄	2.957×10^6	5.080×10^5	2.449×10^6	5.82

Continued

Table B-1 (continued)
(Experiment 6)

Lattice Position	Face	Position on Assembly	A_s Total	A_s Cd	A_s Thermal	Cd Ratio
28	South	℄	3.978×10^6	1.301×10^6	2.677×10^6	3.06
		6" above ℄	3.263×10^6			
		6" below ℄	3.435×10^6	1.050×10^6	2.385×10^6	3.27
		12"above ℄	2.223×10^6			
		12"below ℄	2.117×10^6	4.004×10^5	1.717×10^6	5.29
36	North	℄	6.450×10^6	1.573×10^6	4.877×10^6	4.10
		6" above ℄	5.067×10^6			
		6" below ℄	5.167×10^6	1.311×10^6	3.856×10^6	3.94
		12"above ℄	2.734×10^6			
		12"below ℄	2.899×10^6	4.660×10^5	2.433×10^6	6.22
	South	℄	5.773×10^6	1.152×10^6	4.621×10^6	5.01
		6" above ℄	4.698×10^6			
		6" below ℄	4.790×10^6	9.297×10^5	3.860×10^6	5.15
		12"above ℄	2.342×10^6			
		12"below ℄	2.595×10^6	3.390×10^5	2.256×10^6	7.65
37	North	℄	4.778×10^6	1.562×10^6	3.216×10^6	3.06
		6" above ℄	4.075×10^6			
		6" below ℄	4.099×10^6	1.250×10^6	2.849×10^6	3.28
		12"above ℄	2.639×10^6			
		12"below ℄	2.482×10^6	4.623×10^5	2.020×10^6	5.37
	South	℄	4.932×10^6	1.281×10^6	3.651×10^6	3.85
		6" above ℄	3.951×10^6			
		6" below ℄	4.058×10^6	1.005×10^6	3.053×10^6	4.04

Continued

Table B-1 (continued)
(Experiment 6)

Lattice Position	Face	Position on Assembly	A_s Total	A_s Cd	A_s Thermal	Cd Ratio
37	South	12"above ℄	2.305×10^6			
		12"below ℄	2.037×10^6	4.006×10^5	1.636×10^6	5.08
48	North	℄	3.424×10^6	1.074×10^6	2.350×10^6	3.19
		6" above ℄	2.773×10^6			
		6" below ℄	2.807×10^6	8.510×10^5	1.956×10^6	3.30
		12"above ℄	1.890×10^6			
		12"below ℄	1.720×10^6	3.072×10^5	1.413×10^6	5.60
	South	℄	3.148×10^6	6.995×10^5	2.449×10^6	4.50
		6" above ℄	2.552×10^6			
		6" below ℄	2.557×10^6	5.549×10^5	2.002×10^6	4.61
		12"above ℄	1.524×10^6			
		12"below ℄	1.424×10^6	1.949×10^5	1.229×10^6	7.31
45	North	℄	5.414×10^6	1.157×10^6	4.257×10^6	4.68
		3" above ℄	4.993×10^6			
		3" below ℄				
		6" above ℄	3.697×10^6			
		6" below ℄	4.362×10^6	8.826×10^5	3.479×10^6	4.94
		9" above ℄	2.350×10^6			
		9" below ℄		7.166×10^5		
		12"above ℄				
		12"below ℄	2.186×10^6	3.801×10^5	1.806×10^6	5.75
	South	℄	3.831×10^6	7.061×10^5	3.125×10^6	5.43
		3" above ℄				
		3" below ℄	3.468×10^6			

Continued

Table B-1 (continued)
(Experiment 6)

Lattice Position	Face	Position on Assembly	A_s Total	A_s Cd	A_s Thermal	Cd Ratio
45	South	6" above ℄	2.917×10^6			
		6" below ℄	3.082×10^6	5.452×10^5	2.537×10^6	5.65
		9" above ℄				
		9" below ℄	2.363×10^6	3.967×10^5	1.966×10^6	5.96
		12" above ℄	1.627×10^6			
		12" below ℄	1.594×10^6	2.032×10^5	1.391×10^6	7.84
5 BeO	North	℄	4.838×10^6	5.528×10^5	4.285×10^6	8.75
		6" above ℄	3.921×10^6			
		6" below ℄	4.123×10^6	3.633×10^5	3.760×10^6	11.35
		12" above ℄	2.021×10^6			
		12" below ℄	1.804×10^6	1.781×10^5	1.626×10^6	10.13
6 BeO	North	℄	4.822×10^6			
		6" above ℄	3.823×10^6			
		6" below ℄	4.076×10^6			
		12" above ℄	1.876×10^6			
		12" below ℄	1.833×10^6			
7 BeO	North	℄	4.499×10^6	3.930×10^5	4.106×10^6	11.45
		6" above ℄	3.539×10^6			
		6" below ℄	3.635×10^6	3.179×10^5	3.317×10^6	11.43
		12" above ℄	1.620×10^6			
		12" below ℄	1.462×10^6	1.142×10^5	1.348×10^6	12.80
8 BeO	North	℄	3.294×10^6			
		6" above ℄	2.618×10^6			

Continued

Table B-1 (continued)
(Experiment 6)

Lattice Position	Face	Position on Assembly	A_s Total	A_s Cd	A_s Thermal	Cd Ratio
8 BeO	North	6" below ℄	2.731×10^6			
		12" above ℄	1.282×10^6			
		12" below ℄	1.242×10^6			
9 BeO	North	℄	2.316×10^6	1.991×10^5	2.117×10^6	11.63
		6" above ℄	1.877×10^6			
		6" below ℄	1.910×10^6	1.645×10^5	1.746×10^6	11.61
		12" above ℄	9.781×10^5			
		12" below ℄	8.566×10^5	6.295×10^4	8.503×10^6	13.61

Table B-2

Thermal-Neutron Traverses Through the Divided Shield Reactor
(Experiment 6)

North Side of Lattice Position	A_s Total	A_s Epicadmium	A_s Thermal	nv_{th}	Cd Ratio
05-0	4.838×10^6	5.528×10^5	4.285×10^6	1.264×10^7	8.75
15-0	5.345×10^6	1.450×10^6	3.895×10^6	1.149×10^7	3.69
25-0	5.556×10^6	1.839×10^6	3.717×10^6	1.096×10^7	3.02
35-0	6.764×10^6	1.596×10^6	5.168×10^6	1.525×10^7	4.24
45-0	5.414×10^6	1.157×10^6	4.257×10^6	1.256×10^7	4.68
55-0	3.831×10^6	7.061×10^5	3.125×10^6	9.219×10^6	5.43
05-6	4.022×10^6	3.544×10^5	3.668×10^6	1.082×10^7	11.35
15-6	4.396×10^6	1.195×10^6	3.201×10^6	9.443×10^6	3.68
25-6	4.393×10^6	1.504×10^6	2.889×10^6	8.522×10^6	2.92
35-6	5.411×10^6	1.339×10^6	4.072×10^6	1.201×10^7	4.04
45-6	4.029×10^6	8.156×10^5	3.213×10^6	9.478×10^6	4.94
55-6	2.999×10^6	5.308×10^5	2.468×10^6	7.281×10^6	5.65
05-12	1.912×10^6	1.887×10^5	1.723×10^6	5.083×10^6	10.13
15-12	2.454×10^6	4.765×10^5	1.977×10^6	5.832×10^6	5.15
25-12	2.877×10^6	5.731×10^5	2.304×10^6	6.797×10^6	5.02
35-12	2.748×10^6	4.722×10^5	2.276×10^6	6.714×10^6	5.82
45-12	2.186×10^6	3.801×10^5	1.806×10^6	5.328×10^6	5.75
55-12	1.610×10^6	2.053×10^5	1.405×10^6	4.145×10^6	7.84

Continued

Table B-2 (continued)
(Experiment 6)

Values in Parentheses are Interpolated from the Appropriate Curves

North Side of Lattice Position	A_s Total	A_s Epicadmium	A_s Thermal	nv_{th}	Cd Ratio
06-0	4.822×10^6				
16-0	5.307×10^6	1.399×10^6	3.908×10^6	1.153×10^7	3.79
26-0	6.444×10^6	1.749×10^6	4.695×10^6	1.385×10^7	3.68
36-0	6.450×10^6	1.573×10^6	4.877×10^6	1.439×10^7	4.10
46-0	5.773×10^6	1.152×10^6	4.621×10^6	1.363×10^7	5.01
56-0	H_2O				
06-6	3.949×10^6				
16-6	4.437×10^6	(1.174×10^6)	(3.263×10^6)	(9.626×10^6)	(3.78)
26-6	5.266×10^6	1.435×10^6	3.831×10^6	1.130×10^7	3.67
36-6	5.117×10^6	1.299×10^6	3.818×10^6	1.126×10^7	3.94
46-6	4.744×10^6	9.212×10^5	3.823×10^6	1.128×10^7	5.15
56-6	H_2O				
06-12	1.854×10^6				
16-12	2.432×10^6	4.108×10^5	2.021×10^6	5.962×10^6	5.92
26-12	2.993×10^6	5.482×10^5	2.445×10^6	7.213×10^6	5.46
36-12	2.816×10^6	4.527×10^5	2.363×10^6	6.971×10^6	6.22
46-12	2.468×10^6	3.226×10^5	2.145×10^6	6.328×10^6	7.65
56-12	H_2O				

Continued

Table B-2 (continued)
(Experiment 6)

North Side of Lattice Position	A_s Total	A_s Epicadmium	A_s Thermal	nv_{th}	Cd Ratio
07-0	4.499×10^6	3.930×10^5	4.106×10^6	1.211×10^7	11.45
17-0	4.955×10^6	1.242×10^6	3.713×10^6	1.095×10^7	3.99
27-0	4.812×10^6	1.579×10^6	3.233×10^6	9.537×10^6	3.05
37-0	4.778×10^6	1.562×10^6	3.216×10^6	9.487×10^6	3.06
47-0	4.932×10^6	1.281×10^6	3.651×10^6	1.077×10^7	3.85
57-0	BeO				
07-6	3.587×10^6	3.138×10^5	3.273×10^6	9.655×10^6	11.43
17-6	4.089×10^6	1.033×10^6	3.056×10^6	9.015×10^6	3.96
27-6	3.952×10^6	1.275×10^6	2.677×10^6	7.897×10^6	3.10
37-6	4.087×10^6	1.246×10^6	2.841×10^6	8.381×10^6	3.28
47-6	4.004×10^6	9.911×10^5	3.013×10^6	8.888×10^6	4.04
57-6	BeO				
07-12	1.541×10^6	1.204×10^5	1.421×10^6	4.192×10^6	12.80
17-12	2.180×10^6	3.971×10^5	1.783×10^6	5.260×10^6	5.49
27-12	2.500×10^6	4.883×10^5	2.012×10^6	5.935×10^6	5.12
37-12	2.560×10^6	4.767×10^5	2.083×10^6	6.145×10^6	5.37
47-12	2.171×10^6	4.274×10^5	1.744×10^6	5.145×10^6	5.08
57-12	BeO				

Continued

Table B-2 (continued)
(Experiment 6)

North Side of Lattice Position	A_s Total	A_s Epicadmium	A_s Thermal	nv_{th}	Cd Ratio
08-0	3.294×10^6				
18-0	3.623×10^6	8.984×10^5	2.725×10^6	8.039×10^6	4.03
28-0	3.963×10^6	1.246×10^6	2.717×10^6	8.015×10^6	3.18
38-0	3.978×10^6	1.301×10^6	2.677×10^6	7.897×10^6	3.06
48-0	3.424×10^6	1.074×10^6	2.350×10^6	6.932×10^6	3.19
58-0	3.148×10^6	6.995×10^5	2.449×10^6	7.224×10^6	4.50
08-6	2.674×10^6				
18-6	2.992×10^6	7.073×10^5	2.285×10^6	6.741×10^6	4.23
28-6	3.229×10^6	1.003×10^6	2.226×10^6	6.567×10^6	3.22
38-6	3.349×10^6	1.024×10^6	2.325×10^6	6.859×10^6	3.27
48-6	2.790×10^6	8.454×10^5	1.945×10^6	5.738×10^6	3.30
58-6	2.554×10^6	5.540×10^5	2.000×10^6	5.900×10^6	4.61
08-12	1.262×10^6				
18-12	1.666×10^6	2.805×10^5	1.385×10^6	4.086×10^6	5.94
28-12	2.033×10^6	3.248×10^5	1.708×10^6	5.039×10^6	6.26
38-12	2.170×10^6	4.102×10^5	1.760×10^6	5.192×10^6	5.29
48-12	1.805×10^6	3.223×10^5	1.483×10^6	4.375×10^6	5.60
58-12	1.474×10^6	2.016×10^5	1.272×10^6	3.752×10^6	7.31
09-0	2.316×10^6	1.991×10^5	2.117×10^6	6.245×10^6	11.63
09-6	1.893×10^6	1.630×10^5	1.730×10^6	5.104×10^6	11.61
09-12	9.173×10^5	6.740×10^4	8.499×10^5	2.507×10^6	13.61

Table B-3

Power Distribution within the Divided Shield Reactor
(Experiment 6)

Lattice Position	G Grams of U^{235}	Average nv_{th} per Element	P Power in Watts	Power per Row
12	139.98	6.47×10^6	0.03572	
13	137.55	8.19×10^6	0.04443	
14	138.22	1.005×10^7	0.05479	
15	138.28	8.88×10^6	0.04843	
16	138.54	1.005×10^7	0.05491	
17	138.00	8.19×10^6	0.04458	
18	137.53	6.47×10^6	0.03509	
				0.3179
22	135.02	6.62×10^6	0.03525	
23	134.90	7.96×10^6	0.04235	
24	69.70	1.09×10^7	0.02996	
25	139.48	1.01×10^7	0.05556	
26	69.08	1.09×10^7	0.02970	
27	137.74	7.96×10^6	0.04324	
28	136.48	6.62×10^6	0.03563	
				0.2717
32	137.37	6.20×10^6	0.03359	
33	137.59	8.26×10^6	0.04482	
34	139.95	1.08×10^7	0.05961	
35	69.14	1.035×10^7	0.02822	
36	138.00	1.08×10^7	0.05878	
37	139.98	8.26×10^6	0.04560	
38	138.54	6.20×10^6	0.03388	
				0.3045

Continued

Table B-3 (continued)

(Experiment 6)

Lattice Position	G Grams of U^{235}	Average nv-th per Element	P Power in Watts	Power per Row
42	138.54	5.69×10^6	0.03109	
45	110.21	8.10×10^6	0.03521	
48	136.39	5.69×10^6	0.03061	0.0969
Total	3076.2		0.9910	

Table B-4

Thermal-Neutron Flux Measurements
in the Divided Shield Reactor
(Experiment 7)

Lattice Position	Face	Position on Assembly	A_s Total	A_s Cd	A_s Thermal	nv_{th}	Cd Ratio
15	North	℄	4.280×10^6	1.266×10^6	3.014×10^6	8.891×10^6	3.38
		6" above ℄	3.405×10^6				
		6" below ℄	3.731×10^6	9.841×10^5	2.747×10^6	8.104×10^6	3.79
		12"above ℄	1.949×10^6				
		12"below ℄	2.244×10^6	3.650×10^5	1.879×10^6	5.543×10^6	6.15
	South	℄	4.751×10^6	1.634×10^6	3.117×10^6	9.195×10^6	2.91
		6" above ℄	3.675×10^6				
		6" below ℄	3.978×10^6	1.383×10^6	2.595×10^6	7.655×10^6	2.88
		12"above ℄	2.498×10^6				
		12"below ℄	2.486×10^6	5.062×10^5	1.980×10^6	5.841×10^6	4.91
16	North	℄	4.170×10^6	1.132×10^6	3.038×10^6	8.962×10^6	3.68
		6" above ℄	3.189×10^6				
		6" below ℄	3.551×10^6	9.422×10^5	2.609×10^6	7.696×10^6	3.77
		12"above ℄	1.859×10^6				
		12"below ℄	2.046×10^6	3.311×10^5	1.715×10^6	5.059×10^6	6.18
	South	℄	5.396×10^6	1.506×10^6	3.890×10^6	1.147×10^7	3.58
		6" above ℄	4.548×10^6				
		6" below ℄	4.444×10^6	1.251×10^6	3.193×10^6	9.419×10^6	3.55
		12"above ℄	2.484×10^6				
		12"below ℄	2.538×10^6	4.764×10^5	2.062×10^6	6.083×10^6	5.33

Continued

Table B-4 (continued)
(Experiment 7)

Lattice Position	Face	Position on Assembly	A_s Total	A_s Cd	A_s Thermal	nv_{th}	Cd Ratio
17	North	℄	4.240×10^6	1.075×10^6	3.165×10^6	9.337×10^6	3.94
		6" above ℄	3.444×10^6				
		6" below ℄	3.438×10^6	9.624×10^5	2.476×10^6	7.304×10^6	3.57
		12"above ℄	2.010×10^6				
		12"below ℄	1.722×10^6	3.428×10^5	1.379×10^6	4.068×10^6	5.02
	South	℄	4.592×10^6	1.356×10^6	3.236×10^6	9.546×10^6	3.39
		6" above ℄	3.639×10^6				
		6" below ℄	3.438×10^6	1.111×10^6	2.327×10^6	6.865×10^6	3.09
		12"above ℄	2.281×10^6				
		12"below ℄	2.138×10^6	4.186×10^5	1.719×10^6	5.071×10^6	5.11
18	North	℄	3.131×10^6	7.617×10^5	2.369×10^6	6.988×10^6	4.11
		6" above ℄	2.505×10^6				
		6" below ℄	2.620×10^6	6.380×10^5	1.982×10^6	5.847×10^6	4.11
		12"above ℄	1.291×10^6				
		12"below ℄	1.293×10^6	2.500×10^5	1.043×10^6	3.077×10^6	5.17
	South	℄	3.304×10^6	1.035×10^6	2.269×10^6	6.693×10^6	3.19
		6" above ℄	2.681×10^6				
		6" below ℄	2.813×10^6	8.242×10^5	1.989×10^6	5.867×10^6	3.41
		12"above ℄	1.773×10^6				
		12"below ℄	1.793×10^6	3.016×10^5	1.491×10^6	4.398×10^6	5.94
25	South	℄	6.107×10^6	1.482×10^6	4.625×10^6	1.364×10^7	4.12
		6" above ℄	4.008×10^6				
		6" below ℄	4.931×10^6				

Continued

Table B-4 (continued)

(Experiment 7)

Lattice Position	Face	Position on Assembly	A_s Total	A_s Cd	A_s Thermal	nv_{th}	Cd Ratio
25	South	12"above ℄	2.163×10^6				
		12"below ℄		4.660×10^5		(7.230×10^6)	
36	North	℄	5.851×10^6	1.468×10^6	4.383×10^6	1.293×10^7	3.99
		6" above ℄	4.667×10^6				4.01
		6" below ℄	4.838×10^6	1.207×10^6	3.631×10^6	1.071×10^7	4.01
		12"above ℄	2.513×10^6				
		12"below ℄	2.800×10^6	4.341×10^5	2.366×10^6	6.980×10^6	6.45
	South	℄	4.775×10^6	1.280×10^6	3.495×10^6	1.031×10^7	3.73
		6" above ℄	3.618×10^6				
		6" below ℄	3.896×10^6	1.030×10^6	2.866×10^6	8.455×10^6	3.78
		12"above ℄	2.204×10^6				
		12"below ℄	2.093×10^6	3.732×10^5	1.720×10^6	5.074×10^6	5.61
37	North	℄	4.255×10^6	1.393×10^6	2.862×10^6	8.443×10^6	3.05
		6" above ℄	3.449×10^6				
		6" below ℄	3.528×10^6	1.108×10^6	2.420×10^6	7.139×10^6	3.18
		12"above ℄	2.302×10^6				
		12"below ℄	2.195×10^6	4.500×10^5	1.745×10^6	5.148×10^6	4.88
	South	℄	5.086×10^6	1.346×10^6	3.740×10^6	1.103×10^7	3.78
		6" above ℄	3.708×10^6				
		6" below ℄	4.208×10^6	1.106×10^6	3.102×10^6	9.151×10^6	3.80
		12"above ℄	2.162×10^6				
		12"below ℄	2.353×10^6	4.239×10^5	1.929×10^6	5.690×10^6	5.55

Continued

Table B-4 (continued)

(Experiment 7)

Lattice Position	Face	Position on Assembly	A_s Total	A_s Cd	A_s Thermal	nv_{th}	Cd Ratio
38	North	℄	3.189×10^6	1.109×10^6	2.080×10^6	6.136×10^6	2.875
		6" above ℄	2.729×10^6				
		6" below ℄	2.592×10^6	9.164×10^5	1.676×10^6	4.944×10^6	2.83
		12" above ℄	1.811×10^6				
		12" below ℄	1.632×10^6	3.645×10^5	1.267×10^6	3.738×10^6	4.48
	South	℄	2.599×10^6	7.927×10^5	1.806×10^6	5.328×10^6	3.28
		6" above ℄	2.172×10^6				
		6" below ℄	2.165×10^6				
		12" above ℄	1.489×10^6				
		12" below ℄	1.351×10^6	2.386×10^5	1.112×10^6	3.280×10^6	5.66
45	North	℄	5.402×10^6	1.251×10^6	4.151×10^6	1.224×10^7	4.32
		6" above ℄	3.752×10^6				
		6" below ℄	4.340×10^6	1.051×10^6	3.289×10^6	9.702×10^6	4.13
		12" above ℄	1.790×10^6				
		12" below ℄	2.288×10^6	3.615×10^5	1.926×10^6	5.682×10^6	6.33
	South	℄	3.877×10^6	9.223×10^5	2.955×10^6	8.717×10^6	4.20
		6" above ℄	2.973×10^6				
		6" below ℄	3.285×10^6	6.951×10^5	2.590×10^6	7.640×10^6	4.73
		12" above ℄	1.834×10^6				
		12" below ℄	1.783×10^6	2.664×10^5	1.517×10^6	4.475×10^6	6.69
48	South	℄	2.288×10^6	4.836×10^5	1.804×10^6	5.322×10^6	4.73
		6" above ℄	1.919×10^6				
		6" below ℄	1.959×10^6	3.836×10^5	1.575×10^6	4.646×10^6	5.11
		12" above ℄	1.072×10^6				
		12" below ℄	1.052×10^6	1.347×10^5	9.173×10^5	2.706×10^6	7.81

Table B-5
Thermal-Neutron Traverses Through
the Divided Shield Reactor
(Experiment 7)

Values in Parentheses are Interpolated from the Appropriate Curves

North Side of Lattice Position	A_s Total	A_s Epicadmium	A_s Thermal	nv_{th}	Cd Ratio
15-0	4.280×10^6	1.266×10^6	3.014×10^6	8.891×10^6	3.38
25-0	4.751×10^6	1.634×10^6	3.117×10^6	9.195×10^6	2.91
35-0	6.107×10^6	1.482×10^6	4.625×10^6	1.364×10^7	4.12
45-0	5.402×10^6	1.251×10^6	4.151×10^6	1.224×10^7	4.32
55-0	3.877×10^6	9.223×10^5	2.955×10^6	8.717×10^6	4.20
15-6	3.568×10^6	9.412×10^5	2.627×10^6	7.750×10^6	3.79
25-6	3.826×10^6	1.329×10^6	2.497×10^6	7.366×10^6	2.88
35-6	4.469×10^6	(1.146×10^6)	(3.323×10^6)	(9.803×10^6)	(3.9)
45-6	4.046×10^6	9.797×10^5	3.066×10^6	9.045×10^6	4.13
55-6	3.129×10^6	6.618×10^5	2.467×10^6	7.278×10^6	4.73
15-12	2.096×10^6	3.409×10^5	1.755×10^6	5.177×10^6	6.15
25-12	2.492×10^6	5.075×10^5	1.984×10^6	5.853×10^6	4.91
35-12	(2.54×10^6)	(4.057×10^5)	(2.13×10^6)	(6.283×10^6)	(6.26)
45-12	2.039×10^6	3.221×10^5	1.716×10^6	5.062×10^6	6.33
55-12	1.808×10^6	2.702×10^5	1.538×10^6	4.537×10^6	6.69
16-0	4.170×10^6	1.132×10^6	3.038×10^6	8.962×10^6	3.68
26-0	5.396×10^6	1.506×10^6	3.890×10^6	1.147×10^7	3.58
36-0	5.851×10^6	1.468×10^6	4.383×10^6	1.293×10^7	3.99
46-0	4.775×10^6	1.280×10^6	3.495×10^6	1.031×10^7	3.73
56-0	BeO				

Continued

Table B-5 (continued)

(Experiment 7)

North Side of Lattice Position	A_s Total	A_s Epicadmium	A_s Thermal	nv_{th}	Cd Ratio
16-6	3.370×10^6	8.940×10^5	2.476×10^6	7.304×10^6	3.77
26-6	4.496×10^6	1.266×10^6	3.230×10^6	9.528×10^6	3.55
36-6	4.752×10^6	1.185×10^6	3.567×10^6	1.052×10^7	4.01
46-6	3.757×10^6	9.935×10^5	2.763×10^6	8.151×10^6	3.78
56-6	BeO				
16-12	1.952×10^6	3.159×10^5	1.636×10^6	4.826×10^6	6.18
26-12	2.511×10^6	4.712×10^5	2.040×10^6	6.018×10^6	5.33
36-12	2.656×10^6	4.118×10^5	2.244×10^6	6.620×10^6	6.45
46-12	2.148×10^6	3.830×10^5	1.765×10^6	5.207×10^6	5.61
56-12	BeO				
17-0	4.240×10^6	1.075×10^6	3.165×10^6	9.337×10^6	3.94
27-0	4.592×10^6	1.356×10^6	3.236×10^6	9.546×10^6	3.39
37-0	4.255×10^6	1.393×10^6	2.862×10^6	8.443×10^6	3.05
47-0	5.086×10^6	1.346×10^6	3.740×10^6	1.103×10^7	3.78
57-0	H_2O				
17-6	3.441×10^6	9.635×10^5	2.477×10^6	7.307×10^6	3.57
27-6	3.538×10^6	1.144×10^6	2.394×10^6	7.062×10^6	3.09
37-6	3.488×10^6	1.096×10^6	2.392×10^6	7.056×10^6	3.18
47-6	3.958×10^6	1.041×10^6	2.917×10^6	8.605×10^6	3.80
57-6	H_2O				

Continued

Table B-5 (continued)
(Experiment 7)

North Side of Lattice Position	A_s Total	A_s Epicadmium	A_s Thermal	nv_{th}	Cd Ratio
17-12	1.866×10^6	3.716×10^5	1.494×10^6	4.407×10^6	5.02
27-12	2.209×10^6	4.325×10^5	1.777×10^6	5.242×10^6	5.11
37-12	2.248×10^6	4.608×10^5	1.787×10^6	5.272×10^6	4.88
47-12	2.257×10^6	4.067×10^5	1.850×10^6	5.457×10^6	5.55
57-12	H_2O				
18-0	3.131×10^6	7.617×10^5	2.369×10^6	6.988×10^6	4.11
28-0	3.304×10^6	1.035×10^6	2.269×10^6	6.693×10^6	3.19
38-0	3.189×10^6	1.109×10^6	2.080×10^6	6.136×10^6	2.875
48-0	2.599×10^6	7.927×10^5	1.806×10^6	5.328×10^6	3.28
58-0	2.288×10^6	4.836×10^5	1.804×10^6	5.322×10^6	4.73
18-6	2.562×10^6	6.237×10^5	1.938×10^6	5.717×10^6	4.11
28-6	2.747×10^6	8.052×10^5	1.942×10^6	5.729×10^6	3.41
38-6	2.660×10^6	9.403×10^5	1.720×10^6	5.074×10^6	2.83
48-6	2.168×10^6	(5.86×10^5)	(1.582×10^6)	(4.667×10^6)	(3.7)
58-6	1.939×10^6	3.795×10^5	1.559×10^6	4.599×10^6	5.11
18-12	1.292×10^6	2.498×10^5	1.042×10^6	3.074×10^6	5.17
28-12	1.783×10^6	3.000×10^6	1.482×10^6	4.372×10^6	5.94
38-12	1.721×10^6	3.843×10^5	1.337×10^6	3.944×10^6	4.48
48-12	1.420×10^6	2.508×10^5	1.169×10^6	3.448×10^6	5.66
58-12	1.062×10^6	1.360×10^5	9.260×10^5	2.732×10^6	7.81

Table B-6
Power Distribution within the Divided Shield Reactor
(Experiment 7)

Lattice Position	G Grams of U^{235}	Average nv_{th} per Element	P Power in Watts	Power per Row
12	139.98	5.50×10^6	0.03036	
13	137.55	7.16×10^6	0.03884	
14	138.22	8.12×10^6	0.04426	
15	138.28	7.42×10^6	0.04047	
16	138.54	8.12×10^6	0.04437	
17	138.00	7.16×10^6	0.03897	
18	137.53	5.50×10^6	0.02983	0.2671
22	135.02	5.34×10^6	0.02844	
23	134.90	7.09×10^6	0.03772	
24	69.70	9.64×10^6	0.02650	
25	139.48	8.66×10^6	0.04764	
26	69.08	9.64×10^6	0.02626	
27	137.74	7.09×10^6	0.03852	
28	136.48	5.34×10^6	0.02874	0.2338
32	137.37	4.79×10^6	0.02595	
33	137.59	7.69×10^6	0.04173	
34	139.95	9.05×10^6	0.04995	
35	69.14	9.36×10^6	0.02552	
36	138.00	9.05×10^6	0.04926	
37	139.98	7.69×10^6	0.04245	
38	138.54	4.79×10^6	0.02617	0.2610

Continued

Table B-6 (continued)

(Experiment 7)

Lattice Position	G Grams of U^{235}	Average nv_{th} per Element	P Power in Watts	Power per Row
42	138.54	4.42×10^6	0.02415	
45	139.20	7.90×10^6	0.04337	
48	136.39	4.42×10^6	0.02378	0.0913
Total	3105.2		0.853	

Table B-7
Thermal-Neutron Flux Measurements
in the "Offset Reactor"
(Experiment 11)

Lattice Position	Face	Position on Assembly	A_s Total	A_s Epicadmium	Cd Ratio
14	South	℄	6.208×10^5	1.091×10^5	5.69
		6" above ℄	4.816×10^5		
		6" below ℄	4.983×10^5	0.9174×10^5	5.43
		12"above ℄	2.196×10^5		
		12"below ℄	2.243×10^5	0.3448×10^5	6.50
15	North	℄	5.728×10^5	1.304×10^5	4.39
		6"above ℄	4.696×10^5		
		6"below ℄	4.588×10^5	1.038×10^5	4.42
		12"above ℄	2.565×10^5		
		12"below ℄	2.263×10^5	0.3884×10^5	5.83
	South	℄	5.812×10^5	1.857×10^5	3.13
		6" above ℄	4.543×10^5		
		6" below ℄	4.656×10^5	1.494×10^5	3.12
		12"above ℄	2.908×10^5		
		12"below ℄	2.908×10^5	0.5552×10^5	5.24
16	North	℄	6.208×10^5	1.628×10^5	3.81
		6" above ℄	5.283×10^5		
		6" below ℄	5.123×10^5	1.333×10^5	3.84
		12"above ℄	3.010×10^5		
		12"below ℄	2.508×10^5	0.4721×10^5	5.31
	South	℄	8.659×10^5		
		6" above ℄	6.930×10^5		
		6" below ℄	7.120×10^5	1.792×10^5	3.97
		12"above ℄	3.599×10^5		
		12"below ℄	3.806×10^5	0.6659×10^5	5.71

Continued

Table B-7 (continued)
(Experiment 11)

Lattice Position	Face	Position on Assembly	A_s Total	A_s Epicadmium	Cd Ratio
17	North	℄	6.169×10^5	1.741×10^5	3.54
		6" above ℄	5.048×10^5		
		6" below ℄	5.048×10^5	1.386×10^5	3.64
		12"above ℄	2.906×10^5		
		12"below ℄	2.591×10^5	0.4984×10^5	5.20
	South	℄	6.899×10^5	2.309×10^5	2.99
		6" above ℄	5.619×10^5		
		6" below ℄	5.641×10^5	1.868×10^5	3.02
		12"above ℄	3.733×10^5		
		12"below ℄	3.543×10^5	0.6735×10^5	5.26
18	North	℄	5.434×10^5	1.346×10^5	4.04
		6" above ℄	4.394×10^5		
		6" below ℄	4.455×10^5	1.086×10^5	4.10
		12"above ℄	2.609×10^5		
		12"below ℄	2.310×10^5	0.3878×10^5	5.96
	South	℄	5.876×10^5	1.882×10^5	3.12
		6" above ℄	4.602×10^5		
		6" below ℄	4.839×10^5	1.502×10^5	3.22
		12"above ℄	2.977×10^5		
		12"below ℄	2.948×10^5	0.5793×10^5	5.09
25	South	℄	8.352×10^5	2.025×10^5	4.12
		6" above ℄	5.823×10^5		
		6" below ℄	6.839×10^5	1.697×10^5	4.03
		12"above ℄	3.296×10^5		
		12"below ℄	3.634×10^5	0.6749×10^5	5.38

Continued

Table B-7 (continued)
(Experiment 11)

Lattice Position	Face	Position on Assembly	A_s Total	A_s Epicadmium	Cd Ratio
27	South	℄	8.115×10^5		
		6" above ℄	6.405×10^5		
		6" below ℄	6.637×10^5		
		9" above ℄	4.656×10^5		
		9" below ℄	4.973×10^5	1.551×10^5	3.21
		12"above ℄	4.244×10^5		
		12"below ℄	4.204×10^5		
34	North	℄	5.802×10^5	1.458×10^5	3.98
		6" above ℄	4.535×10^5		
		6" below ℄	4.696×10^5	1.154×10^5	4.07
		12"above ℄	2.469×10^5		
		12"below ℄	2.602×10^5	0.4531×10^5	5.74
	South	℄	4.735×10^5	1.400×10^5	3.38
		6" above ℄	3.781×10^5		
		6" below ℄	3.867×10^5	0.9098×10^5	4.25
		12"above ℄	2.402×10^5		
		12"below ℄	2.429×10^5		
36	North	℄	9.666×10^5	2.507×10^5	3.86
		6" above ℄	7.575×10^5		
		6" below ℄	7.809×10^5	2.025×10^5	3.86
		12"above ℄	3.960×10^5		
		12"below ℄	4.229×10^5	0.7779×10^5	5.44
	South	℄	7.588×10^5	2.434×10^5	3.12
		6" above ℄	5.984×10^5		
		6" below ℄	6.079×10^5	1.946×10^5	3.12
		12"above ℄	3.873×10^5		
		12"below ℄	3.740×10^5	0.6988×10^5	5.35

Continued

Table B-7 (continued)
(Experiment 11)

Lattice Position	Face	Position on Assembly	A_s Total	A_s Epicadmium	Cd Ratio
36	East	℄	7.948×10^5	2.692×10^5	2.95
		3" above ℄	7.834×10^5		
		3" below ℄	7.734×10^5		
		6" above ℄	6.545×10^5		
		6" below ℄	6.420×10^5	2.176×10^5	2.95
		9" above ℄	4.918×10^5		
		9" below ℄	4.624×10^5		
		12"above ℄	4.083×10^5		
		12"below ℄	4.084×10^5	0.7463×10^5	5.47
	West	℄	7.724×10^5	2.416×10^5	3.20
		6" above ℄	5.379×10^5		
		6" below ℄	6.278×10^5	1.917×10^5	3.27
		12"above ℄	3.516×10^5		
		12"below ℄	3.748×10^5	0.6697×10^5	5.60
37	North	℄	8.072×10^5	2.478×10^5	3.26
		3" above ℄	7.348×10^5		
		3" below ℄	7.513×10^5		
		6" above ℄	6.481×10^5		
		6" below ℄	6.396×10^5	2.048×10^5	3.12
		12"above ℄	4.167×10^5		
		12"below ℄	4.040×10^5	0.7390×10^5	5.47

Continued

Table B-7 (continued)
(Experiment 11)

Lattice Position	Face	Position on Assembly	A_s Total	A_s Epicadmium	Cd Ratio
37	South	℄	7.486×10^5	2.490×10^5	3.01
		6" above ℄	6.089×10^5		
		6" below ℄	6.025×10^5	2.046×10^5	2.94
		9" above ℄	4.280×10^5		
		9" below ℄	4.402×10^5	1.446×10^5	3.04
		12"above ℄	3.959×10^5		
		12"below ℄	3.802×10^5	0.7880×10^5	4.82
37	East Side of Center Fuel Plate	℄	7.525×10^5		
		3" above ℄	7.365×10^5		
		3" below ℄	7.405×10^5		
		6" above ℄	5.886×10^5		
		6" below ℄	6.127×10^5		
		9" above ℄	4.357×10^5		
		9" below ℄	4.519×10^5		
		10.5"above ℄	3.382×10^5		
		10.5"below ℄	3.642×10^5		
38	North	℄	6.849×10^5	2.105×10^5	3.25
		6" above ℄	5.741×10^5		
		6" below ℄	5.583×10^5	1.835×10^5	3.04
		12"above ℄	3.517×10^5		
		12"below ℄	3.523×10^5	0.6901×10^5	5.10

Continued

Table B-7 (continued)
(Experiment 11)

Lattice Position	Face	Position on Assembly	A_s Total	A_s Epicadmium	Cd Ratio
38	South	℄	6.368×10^5	2.022×10^5	3.15
		6" above ℄	4.890×10^5		
		6" below ℄	5.282×10^5	1.682×10^5	3.14
		12"above ℄	3.243×10^5		
		12"below ℄	3.237×10^5	0.6312×10^5	5.13
	East	℄	6.007×10^5	1.631×10^5	3.68
		6" above ℄	4.774×10^5		
		6" below ℄	4.979×10^5	1.342×10^5	3.71
		12"above ℄	2.701×10^5		
		12"below ℄	2.419×10^5	0.4580×10^5	5.28
	West	℄	7.592×10^5	2.389×10^5	3.18
		3" above ℄	7.246×10^5		
		3" below ℄	7.135×10^5		
		6" above ℄	6.067×10^5		
		6" below ℄	6.124×10^5	1.991×10^5	3.08
		9" above ℄	4.556×10^5		
		9" below ℄	4.312×10^5		
		12"above ℄	3.669×10^5		
		12"below ℄	3.763×10^5	0.6766×10^5	5.56

Continued

Table B-7 (continued)
(Experiment 11)

Lattice Position	Face	Position on Assembly	A_s Total	A_s Epicadmium	Cd Ratio
44	South	℄	4.365×10^5	1.187×10^5	3.68
		6" below ℄	3.624×10^5	0.9846×10^5	3.68
		12"above ℄	1.900×10^5		
		12"below ℄	1.995×10^5	0.3692×10^5	5.40
45	North	℄	7.716×10^5	1.976×10^5	3.90
		6" above ℄	4.738×10^5		
		6" below ℄	6.380×10^5	1.600×10^5	3.99
		12"above ℄	2.752×10^5		
		12"below ℄	3.665×10^5	0.6410×10^5	5.72
	South	℄	5.809×10^5	1.669×10^5	3.48
		6" above ℄	4.504×10^5		
		6" below ℄	4.742×10^5	1.319×10^5	3.59
		12"above ℄	2.526×10^5		
		12"below ℄	2.623×10^5	0.4876×10^5	5.38
46	South	℄	6.641×10^5	1.809×10^5	3.67
		6" above ℄	5.500×10^5		
		6" below ℄	5.455×10^5	1.469×10^5	3.71
		12"above ℄	3.190×10^5		
		12"below ℄	2.692×10^5	0.5132×10^5	5.24

Continued

Table B-7 (continued)
(Experiment 11)

Lattice Position	Face	Position on Assembly	A_s Total	A_s Epicadmium	Cd Ratio
47	North	℄	7.421×10^5	2.463×10^5	3.01
		3" above ℄	7.149×10^5		
		3" below ℄	7.124×10^5		
		6" above ℄	5.952×10^5		
		6" below ℄	6.026×10^5	2.015×10^5	2.99
		12"above ℄	3.776×10^5		
		12"below ℄	3.828×10^5	0.6409×10^5	5.97
	South	℄	6.431×10^5	1.844×10^5	3.49
		6" above ℄	5.249×10^5		
		6" below ℄	5.219×10^5	1.420×10^5	3.67
		12"above ℄	3.081×10^5		
		12"below ℄	2.788×10^5	0.5184×10^5	5.38
48	South	℄	5.592×10^5	1.487×10^5	3.76
		6" above ℄	4.494×10^5		
		6" below ℄	4.529×10^5	1.328×10^5	3.41
		12"above ℄	2.546×10^5		
		12"below ℄	2.417×10^5	0.4880×10^5	4.95

Table B-8
Thermal-Neutron Traverses Through the
"Offset Reactor"
(Experiment 11)

North Side of Lattice Position	A_s Total	A_s Epicadmium	A_s Thermal	nv_{th}	Cd Ratio
24-0	6.208×10^5	1.091×10^5	5.117×10^5	1.509×10^6	5.69
34-0	5.802×10^5	1.458×10^5	4.344×10^5	1.281×10^6	3.98
44-0	4.735×10^5	1.400×10^5	3.335×10^5	0.9838×10^6	3.38
54-0	4.365	1.187	3.178	0.9375	3.68
24-6	4.899×10^5	0.9022×10^5	3.997×10^5	1.179×10^6	5.43
34-6	4.615×10^5	1.134×10^5	3.481×10^5	1.027×10^6	4.07
44-6	3.824×10^5	0.8998×10^5	2.924×10^5	0.8626×10^6	4.25
54-6	3.624×10^5	0.9846×10^5	2.639×10^5	0.7785×10^6	3.68
24-12	2.219×10^5	0.3414×10^5	1.878×10^5	0.5540×10^6	6.50
34-12	2.535×10^5	0.4416×10^5	2.093×10^5	0.6174×10^6	5.74
44-12	2.415×10^5	$(0.432) \times 10^5$	$(1.983) \times 10^5$	$(0.585) \times 10^6$	(5.59)
54-12	1.947×10^5	0.3605×10^5	1.586×10^5	0.4679×10^6	5.40
15-0	5.728×10^5	1.304×10^5	4.424×10^5	1.305×10^6	4.39
25-0	5.812×10^5	1.857×10^5	3.955×10^5	1.167×10^6	3.13
35-0	8.352×10^5	2.025×10^5	6.327×10^5	1.866×10^6	4.12
45-0	7.716×10^5	1.976×10^5	5.740×10^5	1.693×10^6	3.90
55-0	5.809×10^5	1.669×10^5	4.140×10^5	1.221×10^6	3.48
15-6	4.642×10^5	1.050×10^5	3.592×10^5	1.060×10^6	4.42
25-6	4.599×10^5	1.474×10^5	3.125×10^5	0.9219×10^6	3.12
35-6	6.331×10^5	1.571×10^5	4.760×10^5	1.404×10^6	4.03
45-6	5.559×10^5	1.393×10^5	4.166×10^5	1.229×10^6	3.99
55-6	4.623×10^5	1.288×10^5	3.335×10^5	0.9838×10^6	3.59

Continued

Table B-8 (continued)
(Experiment 11)

North Side of Lattice Position	A_s Total	A_s Epicadmium	A_s Thermal	nv_{th}	Cd Ratio
15-12	2.414×10^5	0.4141×10^5	2.000×10^5	0.5900×10^6	5.83
25-12	2.908×10^5	0.5552×10^5	2.353×10^5	0.6941×10^6	5.24
35-12	3.465×10^5	0.6440×10^5	2.821×10^5	0.8322×10^6	5.38
45-12	3.208×10^5	0.5608×10^5	2.647×10^5	0.7809×10^6	5.72
55-12	2.574×10^5	0.4784×10^5	2.096×10^5	0.6183×10^6	5.38
16-0	6.208×10^5	1.628×10^5	4.580×10^5	1.351×10^6	3.81
26-0	8.659×10^5	$(2.279) \times 10^5$	$(6.380) \times 10^5$	$(1.882) \times 10^6$	(3.80)
36-0	9.666×10^5	2.507×10^5	7.159×10^5	2.112×10^6	3.86
46-0	7.588×10^5	2.434×10^5	5.154×10^5	1.520×10^6	3.12
56-0	6.641×10^5	1.809×10^5	4.832×10^5	1.425×10^6	3.67
16-6	5.203×10^5	1.355×10^5	3.848×10^5	1.135×10^6	3.84
26-6	7.025×10^5	1.769×10^5	5.256×10^5	1.550×10^6	3.97
36-6	7.692×10^5	1.993×10^5	5.699×10^5	1.681×10^6	3.86
46-6	6.031×10^5	1.933×10^5	4.098×10^5	1.209×10^6	3.12
56-6	5.477×10^5	1.476×10^5	4.001×10^5	1.180×10^6	3.71
16-12	2.759×10^5	0.5196×10^5	2.239×10^5	0.6605×10^6	5.31
26-12	3.702×10^5	0.6483×10^5	3.054×10^5	0.9009×10^6	5.71
36-12	4.094×10^5	0.7526×10^5	3.341×10^5	0.9856×10^6	5.44
46-12	3.806×10^5	0.7114×10^5	3.095×10^5	0.9130×10^6	5.35
56-12	2.941×10^5	0.5613×10^5	2.380×10^5	0.7021×10^6	5.24

Continued

Table B-8 (continued)
(Experiment 11)

North Side of Lattice Position	A_s Total	A_s Epicadmium	A_s Thermal	nv_{th}	Cd Ratio
17-0	6.169×10^5	1.741×10^5	4.428×10^5	1.306×10^6	3.54
27-0	6.899×10^5	2.309×10^5	4.590×10^5	1.354×10^6	2.99
37-0	8.093×10^5	2.482×10^5	5.611×10^5	1.655×10^6	3.26
47-0	7.453×10^5	2.476×10^5	4.977×10^5	1.468×10^6	3.01
57-0	6.431×10^5	1.844×10^5	4.587×10^5	1.353×10^6	3.49
17-6	5.048×10^5	1.386×10^5	3.662×10^5	1.080×10^6	3.64
27-6	5.630×10^5	1.864×10^5	3.766×10^5	1.111×10^6	3.02
37-6	6.479×10^5	2.077×10^5	4.402×10^5	1.298×10^6	3.12
47-6	6.022×10^5	2.028×10^5	3.994×10^5	1.178×10^6	2.97
57-6	5.234×10^5	1.426×10^5	3.808×10^5	1.123×10^6	3.67
17-12	2.748×10^5	0.5285×10^5	2.219×10^5	0.6546×10^6	5.20
27-12	3.638×10^5	0.6916×10^5	2.946×10^5	0.8691×10^6	5.26
37-12	4.163×10^5	0.7611×10^5	3.402×10^5	1.004×10^6	5.47
47-12	3.841×10^5	0.7193×10^5	3.122×10^5	0.9210×10^6	5.34
57-12	2.934×10^5	0.5453×10^5	2.389×10^5	0.7047×10^6	5.38

Continued

Table B-8 (continued)
(Experiment 11)

North Side of Lattice Position	A_s Total	A_s Epicadmium	A_s Thermal	nv_{th}	Cd Ratio
18-0	5.434×10^5	1.346×10^5	4.088×10^5	1.206×10^6	4.04
28-0	5.876×10^5	1.882×10^5	3.994×10^5	1.178×10^6	3.12
38-0	6.849×10^5	2.105×10^5	4.744×10^5	1.399×10^6	3.25
48-0	6.368×10^5	2.022×10^5	4.346×10^5	1.282×10^6	3.15
58-0	5.592×10^5	1.487×10^5	4.105×10^5	1.211×10^6	3.76
18-6	4.424×10^5	1.079×10^5	3.345×10^5	0.9868×10^6	4.10
28-6	4.720×10^5	1.466×10^5	3.254×10^5	0.9599×10^6	3.22
38-6	5.662×10^5	1.862×10^5	3.800×10^5	1.121×10^6	3.04
48-6	5.086×10^5	1.620×10^5	3.466×10^5	1.022×10^6	3.14
58-6	4.511×10^5	1.323×10^5	3.188×10^5	0.9405×10^6	3.41
18-12	2.459×10^5	0.4126×10^5	2.046×10^5	0.6036×10^6	5.96
28-12	2.962×10^5	0.5819×10^5	2.380×10^5	0.7021×10^6	5.09
38-12	3.520×10^5	0.6902×10^5	2.830×10^5	0.8348×10^6	5.10
48-12	3.240×10^5	0.6316×10^5	2.608×10^5	0.7694×10^6	5.13
58-12	2.481×10^5	0.5012×10^5	1.980×10^5	0.5841×10^6	4.95

Table B-9
Power Distribution Within the "Offset Reactor"
(Experiment 11)

Lattice Position	Grams of U^{235}	$nv_{th} \times 10^{-6}$ Average Thermal Flux/Element	Power per Element (watts)	Total Power per Row (watts)
15	134.17	0.965	0.005106	
16	139.07	1.270	0.006966	
17	138.10	1.071	0.005833	
18	139.20	0.948	0.005204	0.02311
24	69.87	1.047	0.002885	
25	138.87	1.151	0.006304	
26	69.79	1.543	0.004247	
27	137.19	1.212	0.006558	
28	138.54	1.034	0.005650	0.02564
34	134.09	0.906	0.004791	
35	69.81	1.305	0.003593	
36	138.43	1.414	0.007720	
37	134.12	1.250	0.006612	
38	138.05	1.071	0.005831	0.02855
44	139.07	0.782	0.004289	
45	137.19	1.092	0.005909	
46	139.20	1.167	0.006407	
47	138.43	1.131	0.006175	
48	139.95	0.971	0.005359	0.02814
Total	2413.14		0.1054	

Table B-10
Thermal-Neutron Flux Data on Special Element A-74S in Position 37
(Experiment 11)

All data normalized to 1/10 watt nominal power

Face	Position on Assembly	A_s Total	A_s Epicadmium	A_s Thermal	nv_{th}[a]	Cd Ratio	nv_{th}[b]
North	℄	8.093×10^5	2.482×10^5	5.611×10^5	1.655×10^6	3.26	1.846×10^6
	3" above ℄	7.348×10^5	2.333×10^5[c]	5.015×10^5[c]	1.479×10^6	3.15[c]	1.650×10^6
	3" below ℄	7.513×10^5	2.385×10^5[c]	5.128×10^5[c]	1.513×10^6	3.15[c]	1.687×10^6
	6" above ℄	6.443×10^5	2.065×10^5[d]	4.378×10^5[d]	1.291×10^6	3.12[d]	1.440×10^6
	6" below ℄	6.516×10^5	2.088×10^5	4.428×10^5	1.306×10^6	3.12	1.457×10^6
	9" above ℄	4.656×10^5	1.450×10^5[d]	3.206×10^5[d]	9.458×10^5	3.21[d]	1.055×10^6
	9" below ℄	4.973×10^5	1.551×10^5	3.422×10^5	1.009×10^6	3.21	1.126×10^6
	12"above ℄	4.205×10^5	7.687×10^4[d]	3.436×10^5[d]	1.014×10^6	5.47[d]	1.130×10^6
	12"below ℄	4.122×10^5	7.536×10^4	3.368×10^5	9.936×10^5	5.47	1.108×10^6
South	℄	7.453×10^5	2.476×10^5	4.977×10^5	1.468×10^6	3.01	1.637×10^6
	3" above ℄	7.149×10^5	2.407×10^5[c]	4.742×10^5[c]	1.399×10^6	2.97[c]	1.560×10^6
	3" below ℄	7.124×10^5	2.399×10^5[c]	4.725×10^5[c]	1.394×10^6	2.97[c]	1.554×10^6
	6" above ℄	6.020×10^5	2.027×10^5[d]	3.993×10^5[d]	1.178×10^6	2.97[d]	1.314×10^6
	6" below ℄	6.025×10^5	2.030×10^5	3.995×10^5	1.178×10^6	2.97	1.314×10^6
	9" above ℄	4.280×10^5	1.408×10^5[d]	2.872×10^5[d]	8.472×10^5	3.04[d]	9.449×10^5
	9" below ℄	4.402×10^5	1.446×10^5	2.956×10^5	8.720×10^5	3.04	9.725×10^5
	12"above ℄	3.867×10^5	7.242×10^4[d]	3.143×10^5[d]	9.272×10^5	5.34[d]	1.034×10^6
	12"below ℄	3.815×10^5	7.144×10^4	3.101×10^5	9.148×10^5	5.34	1.020×10^6

Continued

Table B-10 (continued)
(Experiment 11)

Face	Position on Assembly	A_s Total	A_s Epicadmium	A_s Thermal	nv_{th}(a)	Cd Ratio	nv_{th}(b)
East	℄	7.592×10^5	2.389×10^5	5.203×10^5	1.535×10^6	3.18	1.712×10^6
	3" above ℄	7.246×10^5	2.337×10^5(c)	4.909×10^5(c)	1.448×10^6	3.10(c)	1.615×10^6
	3" below ℄	7.135×10^5	2.302×10^5(c)	4.833×10^5(c)	1.426×10^6	3.10(c)	1.590×10^6
	6" above ℄	6.067×10^5	1.970×10^5(d)	4.097×10^5(d)	1.209×10^6	3.08(d)	1.348×10^6
	6" below ℄	6.124×10^5	1.991×10^5	4.133×10^5	1.219×10^6	3.08	1.360×10^6
	9" above ℄	4.556×10^5	1.456×10^5(c)	3.100×10^5(c)	9.145×10^5	3.13(c)	1.020×10^6
	9" below ℄	4.312×10^5	1.378×10^5(c)	2.934×10^5(c)	8.655×10^5	3.13(c)	9.653×10^5
	12"above ℄	3.669×10^5	6.599×10^4(d)	3.009×10^5(d)	8.876×10^5	5.56(d)	9.900×10^5
	12"below ℄	3.763×10^5	6.766×10^4	3.086×10^5	9.104×10^5	5.56	1.015×10^6
West	℄	7.948×10^5	2.692×10^5	5.256×10^5	1.550×10^6	2.95	1.729×10^6
	3" above ℄	7.834×10^5	2.692×10^5(c)	5.142×10^5(c)	1.517×10^6	2.91(c)	1.692×10^6
	3" below ℄	7.734×10^5	2.657×10^5(c)	5.077×10^5(c)	1.498×10^6	2.91(c)	1.670×10^6
	6" above ℄	6.545×10^5	2.219×10^5(d)	4.326×10^5(d)	1.276×10^6	2.95(d)	1.423×10^6
	6" below ℄	6.420×10^5	2.176×10^5	4.244×10^5	1.252×10^6	2.95	1.396×10^6
	9" above ℄	4.918×10^5	1.639×10^5(c)	3.279×10^5(c)	9.673×10^5	3.00(c)	1.079×10^6
	9" below ℄	4.624×10^5	1.541×10^5(c)	3.083×10^5(c)	9.095×10^5	3.00(c)	1.014×10^6
	12"above ℄	4.083×10^5	7.464×10^4(d)	3.337×10^5(d)	9.844×10^5	5.47(d)	1.098×10^6
	12"below ℄	4.084×10^5	7.463×10^4	3.338×10^5	9.847×10^5	5.47	1.098×10^6

Continued

Table B-10 (continued)

(Experiment 11)

Face	Position on Assembly	A_s Total	A_s Epicadmium	A_s Thermal	nv_{th}(a)	Cd Ratio	nv_{th}(b)
East Side of Center Fuel Plate	℄	7.525×10^5	2.451×10^5(c)	5.074×10^5(c)	1.497×10^6	3.07(c)	1.669×10^6
	3" above ℄	7.365×10^5	2.447×10^5(c)	4.918×10^5(c)	1.451×10^6	3.01(c)	1.618×10^6
	3" below ℄	7.405×10^5	2.460×10^5(c)	4.945×10^5(c)	1.459×10^6	3.01(c)	1.627×10^6
	6" above ℄	5.886×10^5	1.949×10^5(c)	3.937×10^5(c)	1.161×10^6	3.02(c)	1.295×10^6
	6" below ℄	6.127×10^5	2.029×10^5(c)	4.098×10^5(c)	1.209×10^6	3.02(c)	1.348×10^6
	9" above ℄	4.357×10^5	1.424×10^5(c)	2.933×10^5(c)	8.652×10^5	3.06(c)	9.649×10^5
	9" below ℄	4.519×10^5	1.477×10^5(c)	3.042×10^5(c)	8.974×10^5	3.06(c)	1.001×10^6
	10.5" above ℄	3.382×10^5	1.041×10^5(c)	2.341×10^5(c)	6.906×10^5	3.25(c)	7.702×10^5
	10.5" below ℄	3.642×10^5	1.121×10^5(c)	2.521×10^5(c)	7.437×10^5	3.25(c)	8.294×10^5

(a) Arnette calibration, CP-2804.

(b) Klema calibration, ORNL-1398.

(c) Cadmium ratio obtained from curve.

(d) Cadmium ratio assumed from symmetry.

Table B-11
Thermal-Neutron Centerline Flux Measurements
for Open Water Reactors

Distance from South Face of Lattice Position (cm)	North Side of Lattice Position	$\frac{nv_{th}}{\text{nominal watt}}$	$\frac{nv_{th}}{\text{watt}}$	Distance from Reactor		$\frac{nv_{th}}{\text{watt}}$
				North Face (cm)	South Face (cm)	
Unit Shield Reactor; Expt. 1 (Power = 0.74 watts/nominal watt)						
38.10	05-0	0.7301×10^7 [a]	0.989×10^7	7.62	45.7	6.979×10^6 [b]
30.48	15-0	0.6385×10^7 [a]	0.865×10^7	10.00	48.1	4.275×10^6 [b]
22.86	25-0	0.8237×10^7 [a]	1.116×10^7	17.70	55.8	9.221×10^5 [b]
15.24	35-0	1.100×10^7 [a]	1.490×10^7	20.00	58.1	5.66×10^5 [b]
7.62	45-0	0.9972×10^7 [a]	1.351×10^7			
0	55-0	0.7416×10^7 [a]	1.005×10^7			
Divided Shield Reactor; Expt. 6 (Power = 0.991 watts/nominal watt)						
38.10	05-0	1.264×10^7 [c]	1.275×10^7	4.9	43.0	7.081×10^6 [d]
30.48	15-0	1.149×10^7 [c]	1.159×10^7	14.9	53.0	7.690×10^5 [d]
22.86	25-0	1.096×10^7 [c]	1.106×10^7	24.9	63.0	1.086×10^5 [d]
15.24	35-0	1.525×10^7 [c]	1.539×10^7			
7.62	45-0	1.256×10^7 [c]	1.267×10^7			
0	55-0	0.922×10^7 [c]	0.930×10^7			

(a) J. L. Meem and E. B. Johnson, Determination of the Power of the Shield-Testing Reactor I. Neutron Flux Measurements in the Water-Reflected Reactor, ORNL-1027 (Aug. 13, 1951).

(b) E. B. Johnson, G. McCammon, and M. P. Haydon, Foil Measurements of Thermal Neutron Intensities in Water at the BSF, ORNL-CF-51-4-156 (April 18, 1951); also J. L. Meem and H. E. Hungerford, The Unit Shield Experiments at the Bulk Shielding Facility, Appendix F, ORNL-1147 (April 30, 1952).

(c) Appendix B, Table B-2, this report.

(d) H. E. Hungerford, Thermal Neutron Counter Data (to be published).

Appendix C

LEAKAGE CALCULATIONS FOR DIVIDED SHIELD REACTOR

H. E. Hungerford

The results of the power determination and thermal flux patterns within the divided shield reactor have been used to calculate the power leakage of fast neutrons from the north face of the active core for this reactor both in water and in place in the shield mockup. The method was the same as that used for the leakage calculations from the Unit Shield Reactor.[11] A brief outline follows:

The leakage from a given face of the reactor is assumed to be given by

$$L = F \int_{Z_o}^{Z_1} P(Z) e^{-Z/\lambda} \, dZ \qquad (1)$$

where F is a factor converting the power produced to the appropriate type of radiation escaping, Z is the centerline distance inward from the given face, P(Z) is a function of the given power density along Z, Z and Z_o are appropriate limits of integration, and λ is the relaxation length of the escaping radiation. L is evaluated for each row of fuel elements. The total leakage is the sum of the leakage from each row.

For calculation purposes, it is assumed that P(Z) has the form

$$P(Z) = P_o + mZ \tag{2}$$

where P_o is the power produced at the north side of a given row of fuel elements, and m is the slope of the power production along Z. P_o can be evaluated from

$$\frac{P_o}{(nv_{th})_o} = \frac{P_M}{(nv_{th})_M} \tag{3}$$

where P_M is the linear power density at the center of a row of fuel elements (= power per row P_r divided by the width of a fuel element, 7.62 cm) and $(nv_{th})_o$ and $(nv_{th})_M$ are the average thermal-neutron flux values at the north face and center of the row, respectively. The values of $(nv_{th})_o$ and $(nv_{th})_M$ are calculated from Tables B-2 and B-5 (Appendix B).

The value of m may be found from

$$m = \frac{P_M - P_o}{3.81}, \tag{4}$$

where 3.81 is the half-width of a row of fuel elements.

If Eq. (2) is substituted in Eq. (1) and integrated, the leakage for a given row of fuel elements is

$$L/F = (P_o\lambda + m\lambda^2)(e^{-Z_o/\lambda} - e^{-Z_1/\lambda}) + m\lambda\,(Z_o\, e^{-Z_o/\lambda} - Z_1\, e^{-Z_1/\lambda}),$$

where the integration limits Z_o and Z_1 refer to the distances of the north and south sides of a given row of fuel elements from the north

face of the active core. As previously, the 9.7-cm value of λ is used.

The calculations and results are given in Tables C-1 and C-2. Figure C-1 shows a plot of P(Z) against Z for each reactor.

The leakages per unit area per watt of power are

D.S.R. in H_2O	1.08×10^{-4}
D.S.R. in shield mockup	9.09×10^{-5}

A comparison with the values obtained from the 5 by 5 configuration, water-reflected reactor, shows that this 7 by 4 beryllium oxide--reflected reactor in H_2O has a leakage from the north face about 36% higher. The leakage from the divided shield reactor in place in the mockup is about 24% higher than that found for the unit shield reactor.

[redacted]

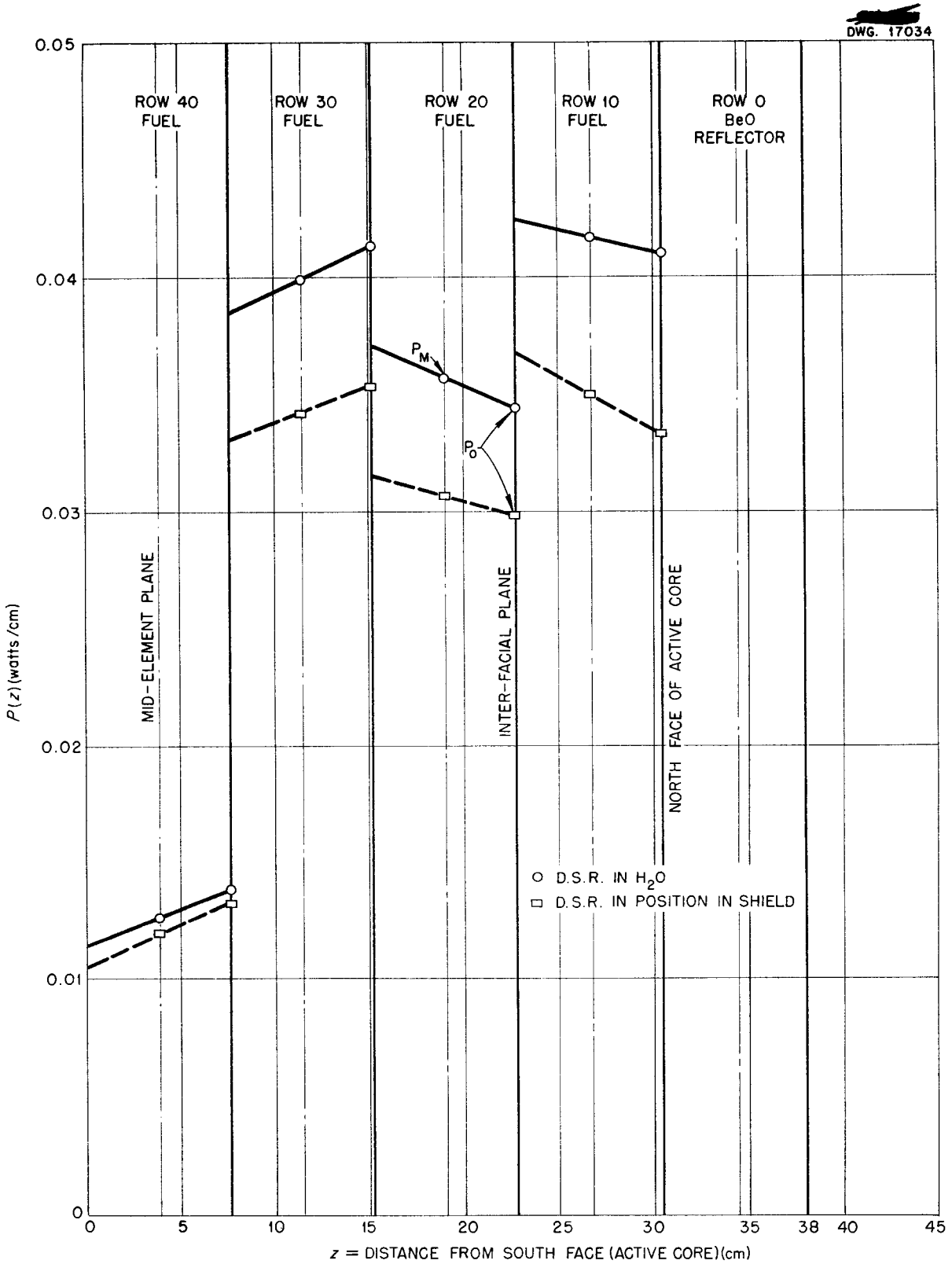

Fig. C-1 $P(z)$ Linear Power Density as a Function of z.

Table C-1

Leakage Calculations for Divided Shield Reactor in Water

(Experiment 11)

Row	$(nv_{th})_o$	$(nv_{th})_M$	P_r (watts)	P_M (watts/cm)	P_o (watts/cm)	m	L/F,[a] Leakage from north face of active core (watts/watt power)
10	8.192×10^6	8.329×10^6	0.31795	0.04172	0.04103	1.811×10^{-4}	0.2198
20	8.467×10^6	8.737×10^6	0.2717	0.03566	0.03456	2.887×10^{-4}	0.0904
30	9.003×10^6	8.697×10^6	0.3045	0.03996	0.04137	-3.701×10^{-4}	0.0380
40	8.387×10^6	7.677×10^6	0.0969	0.01272	0.01390	-3.097×10^{-4}	0.0029
						Total leakage	0.3511

(a) Area of north face of active core = 3252 cm^2;
Leakage per unit area from north face = 1.08×10^{-4} watts/cm^2 per watt of power.

Table C-2

Leakage Calculations for Divided Shield Reactor
in Place in Divided Shield Mockup

(Experiment 7)

Row	$(nv_{th})_o$	$(nv_{th})_M$	P_r (watts)	P_M (watts/cm)	P_o (watts/cm)	m	L/F,[a] Leakage from north face of active core (watts/watt power)
10	6.645×10^6	6.997×10^6	0.2671	0.03505	0.03329	4.619×10^{-4}	0.1838
20	7.348×10^6	7.546×10^6	0.2338	0.03068	0.0987	2.126×10^{-4}	0.0772
30	7.744×10^6	7.490×10^6	0.2610	0.03425	0.03541	-3.045×10^{-4}	0.0327
40	7.237×10^6	6.497×10^6	0.0913	0.01198	0.01334	-3.569×10^{-4}	0.0020
						Total leakage	0.2957

(a) Area of north face of active core = 3252 cm^2;
Leakage per unit area from north face = 9.09×10^{-5} watts/cm^2 per watt of power.

Appendix D

DETERMINATION OF THE THERMAL-NEUTRON FLUX IN SLOTS 1 AND 3 OF THE X-10 STANDARD GRAPHITE PILE

The thermal-neutron flux in slot 11 of the X-10 Standard Graphite Pile has been determined by Klema et al.,[6] who report a thermal flux in that position of 703 neutrons/cm^2/sec. This value is higher than that reported by Arnette and Jones[7] by a factor of 1.0740. It was felt that the thermal flux in the other positions would also be altered but not by the same factor because of the curve fitting method originally used. Therefore, it was recommended that the other exposure positions be recalibrated with reference to slot 11. Recalibration gave values of 1.354×10^4 and 9.466×10^3 neutrons/cm^2/sec for slots 1 and 3, respectively. The calibration procedure follows.

The calibration of slot 11 was done with thin circular gold foils (diameter = 1.25 in.) which were counted on a scintillation counter. Since this counter was not available for the calibration of the other positions, it was necessary to devise other means. The BSF counters require either small gold (1-cm^2) or large indium (25-cm^2) foils, with gold preferred for better correlation with the calibration by Klema. However, the small gold foils could not be sufficiently activated in slot 11 for acceptable counting statistics. It was decided to use larger (25-cm^2) indium foils in slots 1, 3, and 11 to determine the ratio of thermal saturated activities between slot 11 and the two positions nearer the source. The ratio of the thermal saturated activities between slots 1 and 3 measured with the 25-cm^2 indium

foils should be the same as this ratio measured with the 1-cm^2 gold foils, which would also serve as a check on the method.

The foils were exposed in both aluminum and 20-mil cadmium covers along the axis of the pile, the gold foils in slots 1 and 3 and the indium foils in slots 1, 3, and 11. Both sides of the activated foils were counted in gas-flow beta-proportional counters, the saturated activity of a foil being taken as the average of the two sides. A 10% resonance absorption correction was made on the cadmium covered indium foils. The thermal saturated activity is the difference between the total and epicadmium saturated activities. The experimental data is given in Table D-1.

The ratios of the thermal saturated activities observed in slots 1 and 3 were 1.431 for indium and 1.412 for gold. It was felt that this was satisfactory agreement and that the thermal flux in the two positions nearer the source could be determined from the indium exposures.

Since thermal saturated activity is proportional to thermal-neutron flux, the thermal flux in slots 1 and 3 were calculated. For example,

$$nv_{th} \text{ in slot } 1 = nv_{th} \text{ in slot } 11 \left[\frac{A_{s_{th}} \text{ in slot } 1}{A_{s_{th}} \text{ in slot } 11} \right]$$

$$= 703 \left[\frac{2.196 \times 10^5}{1.140 \times 10^4} \right] = 1.354 \times 10^4$$

These values are included in Table D-1, together with those reported in the original calibration. It will be noted that the difference between the old and the new flux values is greater close to the source than it is farther away. This is to be expected because of the "normalization" applied to the original data.

This method of calibration could be easily extended to the other available exposure positions in the Standard Pile.

Table D-1

Foil Data from the X-10 Standard Graphite Pile

Slot Number	A_s Total	A_s Epicadmium	A_s Thermal	Cadmium Ratio	nv_{th}, Arnette-Jones Values	Recalibrated Values[a]
25-cm^2 Indium Foils						
1	2.758×10^5	5.618×10^4	2.196×10^5	5.40	1.2149×10^4	1.354×10^4
3	1.758×10^5	2.229×10^4	1.535×10^5	7.89	8.570×10^3	9.466×10^3
11	1.140×10^4	----	1.140×10^4	300	6.54×10^2	7.03×10^2
1-cm^2 Gold Foils						
1	5.347×10^3	1.228×10^3	4.119×10^3	4.35		
3	3.335×10^3	4.180×10^2	2.917×10^3	7.98		

(a) Based on nv_{th} of 703 neutrons/cm^2/sec in slot 11 as reported by E. D. Klema, R. H. Ritchie, and G. McCammon, Recalibration of the X-10 Standard Graphite Pile, ORNL-1398 (Oct. 17, 1952).

Appendix E

CALIBRATION OF COUNTERS AND FOILS

All thermal flux measurements inside the lattices of the Bulk Shielding Facility reactors have been made with 1-cm^2 gold foils 5 mils in thickness. The foils are cut with a die punch so that the area of each is the same. The thickness is such that, for beta-counting, the detector sees only the side of the foil nearest it. Therefore, variations in thickness are not nearly as important as they would be with thin foils. However, the actual weight variation is kept to approximately $\pm 3.5\%$, which is less than a ± 0.2-mil variation in thickness. Foils of these dimensions are relatively rugged, easy to handle, and can be sufficiently activated in short exposure times at low power levels.

Before a foil can be used to measure an unknown flux, the counters which will be used to measure the induced activity must be calibrated for the particular foil material and geometry. This can be done in several different ways. The method used by the Bulk Shielding Facility group depends on the calibration of the Standard Graphite Pile,[7] where the response of a particular foil to a known thermal-neutron flux can be determined. Several foils of the dimensions and material to be used in the measurement of the unknown flux are exposed to a known flux in the Standard Pile. Both sides of each foil are counted in all counters; in this case, in two mica-window G-M counters and in three gas-flow beta proportional counters. Because of differences in counter efficiency and in counting geometry, the chances are excellent that one will have as

many different values of saturated activity for a specific foil as counters in which the foil was counted.

The Bulk Shielding Facility group has found it convenient to obtain a factor for each counter and, for the end-window tubes, for each counting position in the counter, which will effectively convert the counting rates (and therefore, the saturated activities) of all counters to that of one of the group. This factor is simply the ratio of the observed saturated activity of a foil counted in, for example, counter A, to that observed in the counter, say counter B, which has been chosen as the reference for determining counter factors. Once this has been done for a number of foils, the factors for all counters (each probably different) should be known. This method of calibration eliminates the necessity of determining an "nv_{th} factor" for each counter and simplifies counting in that it makes no difference in which counter a particular foil is counted; all are equivalent after the "counter factor" has been used. It should be kept in mind that both "counter factors" and "nv_{th} factors" must be determined not only for foils of different geometries but also for foils of different materials.

Since the object is to measure thermal flux, the response of the foils to be used to a known thermal flux must be determined. This can be done by exposing the foils, both bare and in cadmium covers, in the Standard Pile in a position where the thermal flux is known. The thermal saturated activity is the difference between the total and cadmium covered (epicadmium) saturated activities. Since

the thermal saturated activity is proportional to the thermal flux, the constant of proportionality, "nv_{th} factor," is the ratio of the thermal saturated activity of a foil (actually the average of several foils) exposed in the Standard Pile to the thermal flux in the exposure position,[7]

$$\frac{nv_{th}\ (\sigma\ \text{pile})}{As_{th}\ (\sigma\ \text{pile})}$$

To measure an unknown thermal flux, it is now simply necessary to determine the <u>thermal</u> saturated activity of "calibrated" foils and multiply this value by the nv_{th} factor.

Obviously, the nv_{th} factor depends not only on the material and geometry of the foil but also on the counter calibration. For earlier work[1] this factor was 9.0 for the 1-cm^2 gold foils. Since that time the counters have been recalibrated using a more sensitive one as the reference. The nv_{th} factor is now 2.95 for the 1-cm^2 5-mil-thick gold foils used in these power determinations, based on the Arnette-Jones calibration of the Standard Pile.

The results of the recalibration of the Standard Pile by Klema et al.[6] became available after the calculations for the reactors described in this report were completed. Using those results together with those in Appendix D, the nv_{th} factor for 1-cm^2 5-mil-thick gold foils is now 3.29.

A discussion of foil techniques is incomplete without a brief discussion of the errors or uncertainties that may be encountered, particularly when foil measurements are made on a mass production basis.

These errors can occur for several reasons, all of which must be eliminated, if possible, or at least reduced to a minimum.

The approach to this problem used by the Bulk Shielding Facility group is described below.

Since a large number of foils are used, it is mandatory that each foil show the same response to a given flux. The purest available material is used for making the foils and, as a final check on effective purity, the half-life of the decay is checked at several levels of activation. Also, the physical dimensions and weight of all the foils are held essentially constant. Counting errors (or deviations) are minimized by taking a minimum of four "counts" on each foil (two counts on each side) and averaging the saturated activities (each of these counts could show a statistical standard deviation of approximately 1%, based on the total number of counts).[12] Since each foil is "counted" (both sides) on at least two different counters, this pattern of counting permits a running check on the constancy of the "counter factors" for all counters. It is felt that deviations in counting geometry are minimized by placing the foil to be counted in a slot milled to fit the foil snuggly but without warpage of the foil. In addition to daily performance checks on the counters, periodic foil exposures are made in the Standard Pile.

Errors in the positioning of foils for exposure are not impossible. Positioning is particularly important when a foil is to be exposed in a strong flux gradient, such as for measuring neutron attenuations in water or for flux measurements at an interface between different media. The exposure positions of foils to be placed on fuel elements are determined

by means of rigid metal strips the length of the fuel elements with holes slightly larger than foil dimensions cut at intervals corresponding to the desired spacing. In this way it is relatively simple to duplicate exposure positions from element to element and between runs.

Appendix F

LINEARITY OF REACTOR CONTROLS

The power of the Bulk Shielding Reactor can be varied to provide a convenient flux for the particular experiment underway. The reactor has been operated in the range from 10^{-1} to 10^{-5} watts, and the linearity of the reactor controls has proved to be excellent. The controls are described in ORNL-991. (13)

A typical experiment for checking the linearity of the reactor controls involved the use of a 3-in. fission chamber. This chamber was placed at a convenient (re counting rate) distance from the reactor and a count was taken at a given reactor power. The power was then raised a factor of 10 and the chamber count was repeated. This procedure was duplicated for each change in the reactor power by a factor 10. Since the fission chamber will suffer counting losses if subjected to too high a flux, it was moved back in the water from the reactor as the power was increased. Table F-1 shows the counting rates obtained in changing the reactor power from 0.1 watt to 10 kw.

When the power was changed by a factor of 10^5, the combined fission chamber readings indicated a discrepancy of about 1.5%. Since the fission chamber is in itself subject to counter losses at the high counting rates, there is no reason to believe that the results from the fission chamber are more dependable than the results from the reactor control settings. Therefore, it has been assumed that the power settings are correct within 1.5% over a range of 10^5 under ordinary conditions.

There are certain conditions under which this accuracy cannot be expected. If the reactor has been operated continuously at maximum power, the power cannot be reduced to less than 1% of maximum with accuracy unless there is a waiting period of about 24 hr. During this waiting period, the gamma radiation in the reactor will decay to a level where the control chambers can compensate for the gamma rays at the lower powers. If the reactor is surrounded with a beryllium oxide reflector and is operated continuously at maximum power, the waiting period before it can be set accurately at 10^{-5} of maximum power is on the order of a month. This effect is due to the photoneutrons from beryllium. In Table F-2 are presented data taken a day after the reactor, with a beryllium oxide reflector on four sides, had been operated at 100 kw. This data was obtained in a manner similar to that described above.

It can be seen that the power was changed from 1 to 100 kw with reasonable accuracy, but that there was a 4% error between 100 watts and 1 kw and below 100 watts the power setting was meaningless. The conclusion is that a research reactor to be operated over a wide range of powers should not have a beryllium or beryllium containing reflector if precise power changes are to be made.

Table F-1

Counting Rates Obtained as Power of Reactor Changes

from 0.1 to 10^4 watts

Run No.	Reactor Power (watts)		Fission Chamber Reading (counts/min)	
1A	0.1		3432	
	0.1		3404	
	0.1		3442	
		Avg.	3426	
				Ratio: 34021/3426 = 9.930
1B	1.0		34057	
	1.0		34005	
	1.0		34001	
		Avg.	34021	
2A	1.0		1179	
	1.0		1192	
	1.0		1170	
		Avg.	1180	
				Ratio: 11808/1180 = 10.007
2B	10.0		11786	
	10.0		11825	
	10.0		11814	
		Avg.	11808	
3A	10.0		2413	
	10.0		2435	
	10.0		2415	
		Avg.	2421	
				Ratio: 24098/2421 = 9.954
3B	10^2		24080	
	10^2		24087	
	10^2		24126	
		Avg.	24098	

Table F-1 (continued)

Run No.	Reactor Power (watts)		Fission Chamber Reading (counts/min)	
4A	10^2 10^2 10^2		1040 1077 1054	
		Avg.	1057	Ratio: 10593/1057 = 10.022
4B	10^3 10^3		10632 10554	
		Avg.	10593	Ratio: 105075/10593 = 9.919
4C	10^4 10^4		104934 105217	
		Avg.	105075	Grand ratio from 0.1 to 10^4 watts = 0.983×10^5

Table F-2

Counting Rates Obtained as Power of Reactor Changes

from 10 to 10^5 watts

Run No	Reactor Power (nominal watts)		Fission Chamber Reading (counts/min)	
1A	10		7669	
	10		7764	
	10		7713	
		Avg.	7715	
				Ratio: 143701/7715 = 18.6
1B	10^2		144465	
	10^2		143677	
	10^2		142962	
		Avg.	143701	
2A	10^2		4822	
	10^2		4600	
	10^2		4636	
		Avg.	4686	
				Ratio: 48804/4686 = 10.41
2B	10^3		49168	
	10^3		48148	
	10^3		49095	
		Avg.	48804	
3A	10^3		6047	
	10^3		6013	
		Avg.	6030	
				Ratio: 60903/6030 = 10.10
3B	10^4		60854	
	10^4		60952	
		Avg.	60903	
4A	10^4		9103	
	10^4		9183	
	10^4		9110	
		Avg.	9132	
				Ratio: 92545/9132 = 10.13
4B	10^5		91254	
	10^5		93075	
	10^5		93305	
		Avg.	92545	

Appendix G

TIME DECAY OF NEUTRONS AND GAMMA RAYS FROM THE BERYLLIUM OXIDE--REFLECTED REACTOR

The time decay of the neutrons and gamma rays from the beryllium oxide--reflected reactor after scram is shown in Figs. G-1 and G-2. Figure G-1 illustrates the decay through several hours, and Fig. G-2 has the time scale expanded to show the shape of the curve in the first few minutes. The reactor was operated for 16 hr at 100 kw of power before scram for one set of decay curves. The next day the reactor was held at 1 kw for 2 hr before scram to obtain the other set of curves. In both cases the reactor had a beryllium oxide reflector on four sides (see Fig. A-5 in Appendix A).

The neutron data was taken from the Log N recorder and the gamma data from the gamma recorder. All data are normalized to unity at the time of scram.

It is interesting to note how quickly the photoneutrons from the beryllium in the reflector appear. The effect is particularly noticeable after shutdown from the lower power. Without the beryllium oxide reflector only the delayed neutrons from the reactor are left after shutdown and these decay in a matter of minutes.

[redacted]

[redacted]

DWG. 17500

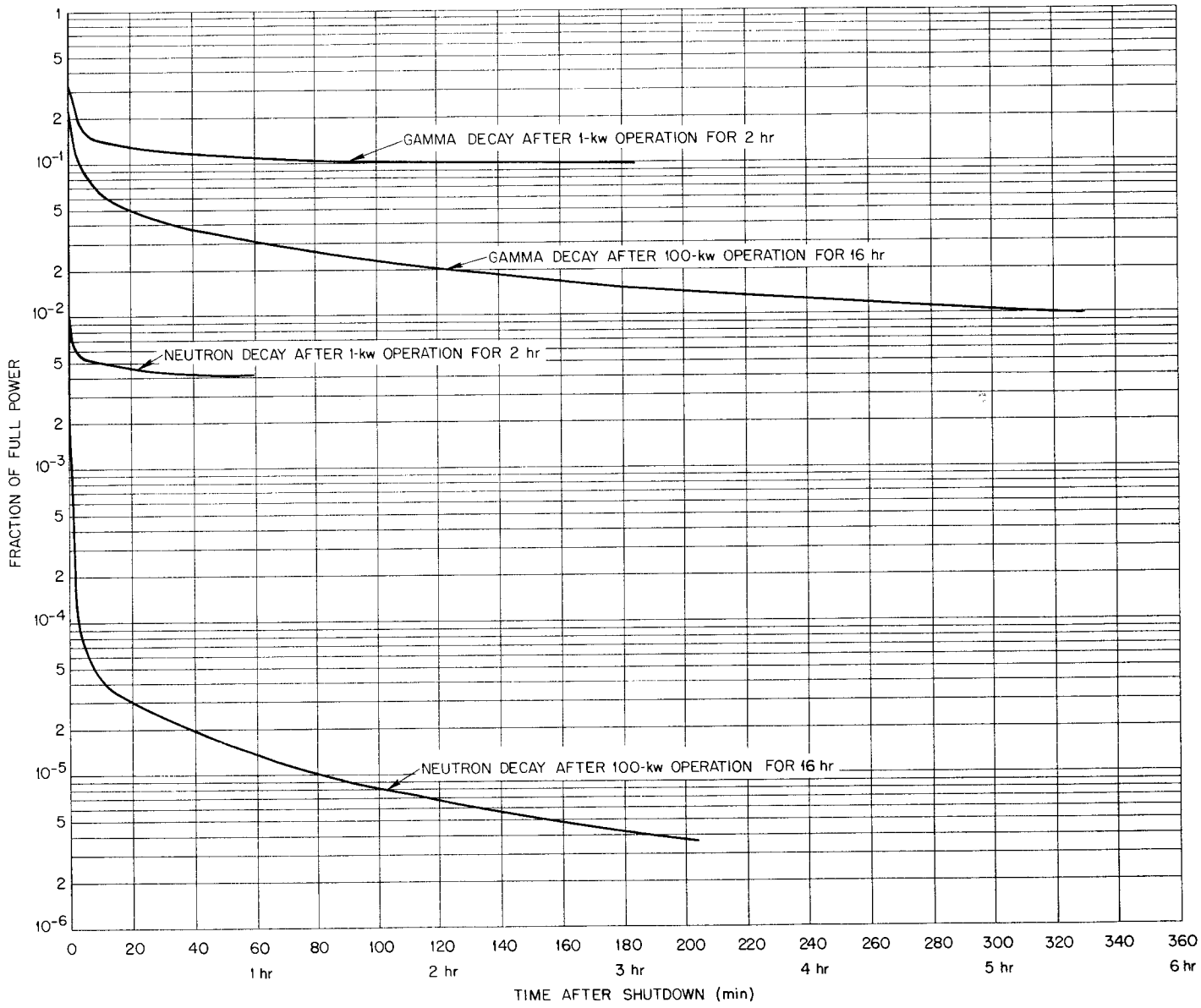

[redacted]

Fig. G-1. Decay of Neutrons and Gamma Rays after Shutdown.

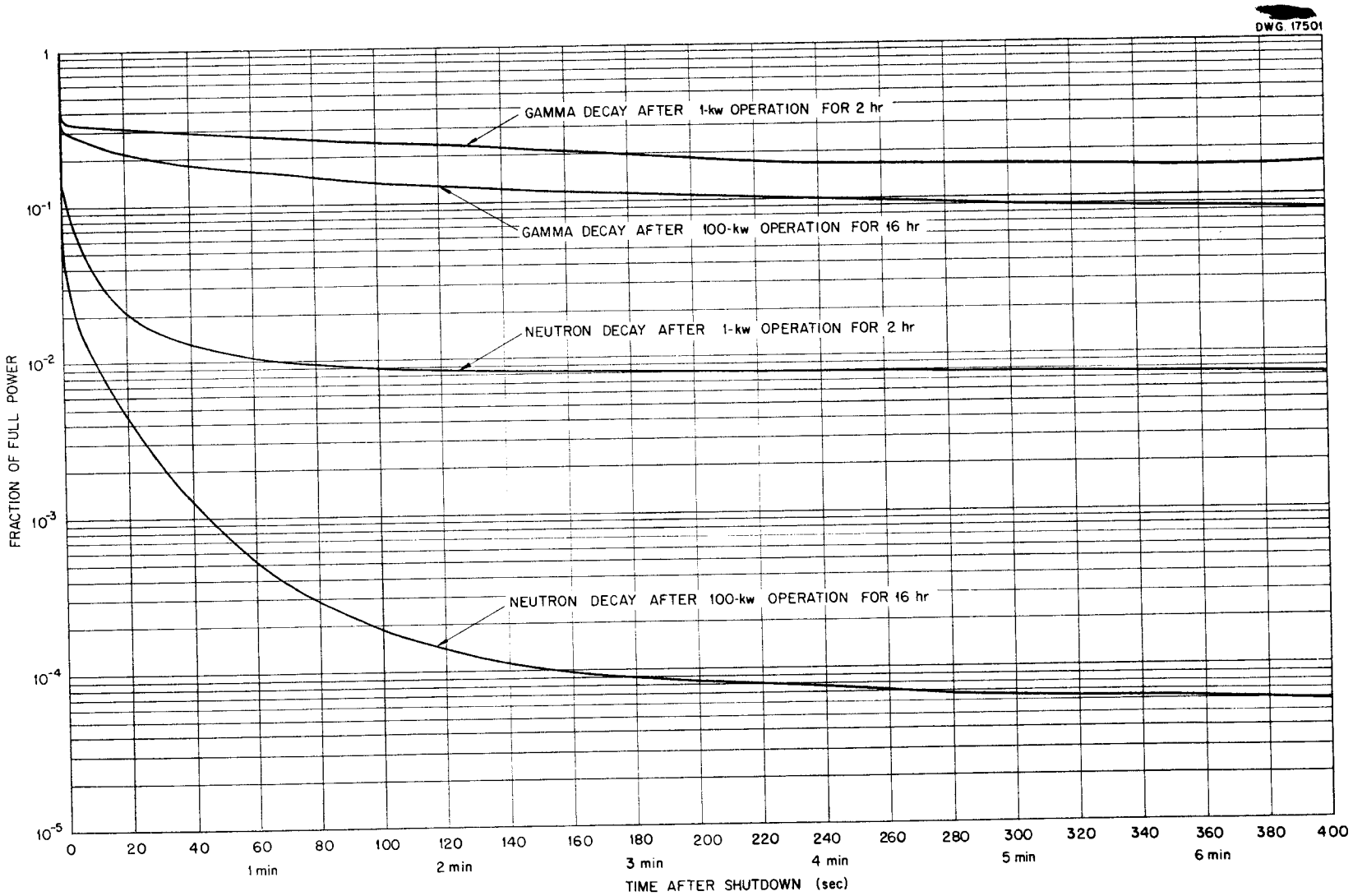

Fig. G-2. Decay of Neutrons and Gamma Rays after Shutdown.

[redacted]

References

1. J. L. Meem and E. B. Johnson, Determination of the Power of the Shield Testing Reactor - I. Neutron Flux Measurements in the Water Reflected Reactor, ORNL-1027 (Aug. 13, 1951).

2. J. L. Meem and H. E. Hungerford, The Unit Shield Experiments at the Bulk Shielding Facility, ORNL-1147 (May 14, 1952).

3. Ibid, Appendix C; also E. B. Johnson, Power Calculations of the Unit Shield Reactor, ORNL-CF-51-9-112 (Sept. 18, 1951).

4. To be published; a tentative experimental program was given in Aircraft Nuclear Propulsion Program Quarterly Progress Report for Period Ending March 10, 1952, ORNL-1227, p. 73 (May 7, 1952).

5. J. L. Meem, L. B. Holland, and G. McCammon, Determination of the Power of the Bulk Shielding Reactor - III. Measurement of the Heat Release per Fission, to be published.

6. E. D. Klema, R. H. Ritchie, and G. McCammon, Recalibration of the X-10 Standard Graphite Pile, ORNL-1398 (Nov. 11, 1952).

7. T. Arnette and H. Jones, Thermal Neutron Flux Distribution in a Standard Graphite Pile, CP-2804 (Apr. 30, 1945).

8. E. D. Klema and R. H. Ritchie, Preliminary Results of the Determination of Thermal Neutron Flux in Water, ORNL-CF-51-4-103 (Apr. 24, 1951); also ORNL-1147, op. cit., Appendix L.

9. ORNL-1147, op. cit., App. F; also E. B. Johnson, G. McCammon, and M. P. Haydon, Foil Measurements of Thermal Neutron Intensities in Water at the Bulk Shielding Facility, ORNL-CF-51-4-156 (Apr. 18, 1951).

10. H. E. Hungerford, Thermal Neutron Counter Data, to be published.

11. H. E. Hungerford and J. L. Meem, Calculations of Leakage from the Bulk Shielding Reactor, ORNL-CF-51-10-94 (Oct. 5, 1951); also ORNL-1147, op. cit., Appendix D.

12. E. R. Cohen, Statistics of Foil Counting, NAA-SR-100 (Sept. 11, 1950).

13. W. M. Breazeale, The New Bulk Shielding Facility at Oak Ridge National Laboratory, ORNL-991 (May 8, 1951).